Doctoral Thesis

NUMERICAL ANALYSIS
OF CONCRETE-FILLED TUBES WITH STIFFENING PLATES
UNDER LARGE DEFORMATION AXIAL LOADING

phD student
Albert Albareda Valls

Directed by
Dr. Jordi Maristany Carreras

June 2012

Chapter V

CALIBRATION OF THE MODEL

❉❉❉

Chapter V is devoted to the validation of the Finite Element Model. Once its geometrical and material features have been described in Chapter IV, it is strictly necessary to check the accuracy of the results obtained in the FE analysis with experimental curves.

Apart from calibrating the finite element model, this chapter is also oriented to describe the behavior of concrete-filled tubes under large deformation axial loading. The understanding of the axial response in these sections is crucial in order to analyze the behavior of reticulated CFT sections.

Therefore, the focus of this description has been directed to the process of confinement effect on concrete core. Different periods coinciding with different load transferences from steel to the core, and in reverse, have been detected and widely described in this Chapter.

Both tensional and damage evolutionary analyses are presented in the Sections shown below, with the final purpose of describing the validity of CFT sections at each stage of loading. This analysis is clearly determinant in order to be capable of conceiving the final conclusions of this work.

❉❉❉

Chapter V

CALIBRATION OF THE MODEL

5.1 Results obtained from the FE Model.

5.1.1 Differences in the stress range of components.
5.1.2 Influence of the geometric nonlinearities on results.
5.1.3 Tensional analysis against damage analysis.

5.2 Verification of the Finite Element Model.

5.2.1 Calibration of the peak and post-peak behavior.
5.2.2 Calibration of large deformation axial loading behavior.

5.3 Description of compressive behavior of circular concrete-filled tubes.

5.3.1 Description of the complete axial load-strain diagram.
5.3.2 Description of the softening branch of the specimens analyzed.
5.3.3 Description of behavior of components in the loading process.
5.3.4 Evolutionary compressive damage description of concrete core.
5.3.5 Description of ductility and mode of failure.
5.3.6 Evolutionary description of contact pressure between components.

5.4 Description of behavior of rectangular concrete filled tubes.

5.4.1 Description of the complete axial load-strain diagram.
5.4.2 Description of the softening branch of the specimens analyzed.
5.4.3 Description of behavior of components in the loading process.
5.4.4 Evolutionary compressive damage description of concrete core.
5.4.5 Description of ductility and mode of failure.
5.4.6 Evolutionary description of contact pressure between components.

5.1 Results obtained from the FE[1] Model.

In this Chapter, the results obtained in a complete study of different concrete-filled tubes [circular and rectangular] are presented. This Chapter has the double purpose of calibrating the FEM model and also providing a general description of the compressive behavior of these typologies. The description of behavior of CFT sections is one of the principal objectives of this investigation, being at the same time a great help for verifying the conclusions presented in Chapters VI, VII and VIII.

A finite element analysis of CFT sections is strictly necessary to be capable of understanding the behavior of each component and the interaction between them, assuming that this is a problem of certain complexity. The FE Models have been done according to all geometrical and material requirements exposed in Chapter IV; although each variable has been calibrated separately before, it is also important to determine the validity of the models as a whole, through a detailed comparison with experimental tests.

5.1.1 Differences in the stress range of components.

The important difference in the stress range of the two components is a true inconvenient to represent the results clearly. The spectrum of colors which corresponds to the stress state of the core and the tube -useful to understand the loading process- is not valid to illustrate the behavior of the composite section as a whole: while in concrete stress varies from 30 to 60 MPa, in steel it goes from 250 up to 450 MPa.

This difference leads to think about the method of representation, usually based on separating the diagrams by components. In case of pretending to represent the behavior of the components in a unique figure, stress variations in concrete would not be appreciated correctly, since the magnitude of these values is really different from those of steel.

5.1.2 Influence of geometrical nonlinearities on results.

Obviously, geometrical nonlinearities are much more important in rectangular sections than in circular sections, as it has been previously explained in Chapter III. This is the reason why an appropriate election of the size of the specimens, the boundary conditions and the used element mesh size[2] is very important. Major geometrical nonlinearities appear in the plastic range of steel, as the specimens are clearly thick-walled; these nonlinearities have also an explicit influence on the concrete core. The use of a coarse mesh for modeling the steel tube leads to false or inaccurate results, mainly owing to the importance of a high density of integration points in elements.

 5.1.3 Tensional analysis against damage analysis.

The loading response of concrete under compression requires an evolutionary damage analysis, always parallel to the tensional. The fact of representing the behavior of concrete core under a tensional point of view only would be not enough, as concrete over all is a cohesive material. These typology of materials do show a serious stiffness degradation during the loading process due to *crushing*, as it has been explained in Chapters II and IV of this study. Although concrete core can resist really high stress levels at advanced strain percentages, provided that being contained in a steel tube, the material at these stages is already completely damaged, not capable of being reloaded again.

---

[1] FE: Finite Element
[2] See Chapter IV for all these considerations.

5.2 Verification of the Finite Element Model.

To verify that the model used for analyzing the proposed specimens is sufficiently accurate for the purpose of this investigation, a minimum of eight different specimens have been calibrated by using their corresponding experimental curves. Experimental results come from several invesigations, all them summarized in the paper "*Uniaxial stress-strain relationship of concrete confined by various shaped steel tubes*", written by (Susanta, et al., 2000). These experimental results have been also used in many other occasions by other researchers such as (Hatzigeorgiou, 2008).

These specimens have been chosen for calibration purpose, so that they have all different combinations of plate thicknesses, material strengths and diameters. The election has been made by using the available samples in the list provided by (Susantha, et al., 2000), from renowned experimental campaigns. In case of circular CFT sections of Table V.1, also a thin-walled specimen has been added to the list in order to guarantee the robustness of the model also for the case of geometrical nonlinearities.

Material and geometrical properties of the circular concrete-filled tubes which have been analyzed are the following:

Table V.1. Geometrical and material features of circular CFT sections used for calibration.

Section	D*	t*	D/t	fy**	fc**	fy/fc	φ	η_1
3MN	150.00	3.20	46.87	287.7	22.0	14.57	1.499	1.788
4HN	150.00	4.00	37.50	279.9	28.70	13.53	1.580	2.230
CC4-C-4	300.20	2.96	101.42	283.0	40.5	6.45	0.964	-0.522
CF4-CC40	318.50	7.90	40.32	358.1	47.5	10.58	1.444	2.374

All values expressed in mm* and N/mm^2**

being:

φ *The effective increment of compressive strength of concrete*

η_1 *Scalar parameter of equation (2.81) of the Eurocode.*

Note that section CC4-C-4 is clearly thin-walled, while the rest are thick-walled.
Thus, these two parameters are related by the following expression:

$$\varphi = \left[1 + \eta_1 \cdot \frac{t}{D} \cdot \frac{f_y}{f_c}\right] = \frac{f_{cc}}{f_c} \tag{5.1}$$

The nomenclature of these specimens comes directly from the paper of (Susanta, et al., 2000), and it responds to the criteria used by researchers who carried out these tests. This nomenclature will be used in the rest of this text.

General features of rectangular sections which have also analyzed are described in Table V.2:

Table V.2. Geometrical and material features of rectangular CFT sections.

Section	B*	t*	B/t	fy**	fc**	fy/fc	φ	η_1
S5	126.80	7.47	16.97	347.0	23.8	14.57	1.261	0.303
S3	126.90	4.55	27.89	322.0	23.8	13.53	1.179	0.368
CR4-A-4	148.20	4.38	33.83	261.2	40.5	6.45	1.051	0.267
4LN	150.00	4.00	34.90	279.9	18.1	15.46	1.142	0.304

All values expressed in mm* and N/mm²**.

Specific conditions of the models considered [mesh size, domain and boundary conditions] and the constitutive material models used in this investigation have been accurately described in Chapter IV. The two most sensitive parts of the load-strain curves are: the *peak of load*[3], and the subsequent behavior corresponding to the softening period. Most sections do show a significative descending branch after the peak of load, due to a low D/t ratio. The determination of the maximum strength of confined concrete and the description of the descending slope during the softening period are two of the most difficult aspects to be calibrated, before assuming the validity of the model.

Since the analysis presented in this investigation is based on large deformation axial loading, until reaching the final collapse, the verification of the model through experimental tests, beyond the softening period is required too. The model also incorporates the hardening for steel at advanced percentages of deformation, using the true stress-strain diagram [strictly necessary in these cases[4]]. In the following Sections 5.2.1 and 5.2.2, the results from this calibration process are shown.

5.2.1 Calibration of the peak and post-peak behavior.

The FE models of the specimens used by Susantha and Ge (Susanta, et al., 2000), mentioned in the previous Section, have been subjected to pure compression tests in order to check their validity. Two families of results [coming from the two different constitutive models described for concrete in Section 4.4.2] have been compared in the analysis. Firstly, these sections have been analyzed by assuming the Drucker Praguer yield Criterion [an elastic perfectly-plastic model], and using ANSYS software; secondly, they have been analyzed by assuming the Damaged Plasticity model for concrete [DPC], available in ABAQUS software.

Results speak by themselves: while the two models reach similar values for the *peak* of load, there is an explicit difference in the post-peak behavior. The blue curve of axial load-strain does not show material degradation after the *peak*, since it corresponds to an elastic perfectly-plastic constitutive model for concrete. Contrarily, the red curve coincides surprisingly with the experimental curve, with a clear descent after this point, as it corresponds to the damaged plasticity model. This material model has been calibrated in order to achieve the maximum coincidence as possible with experimental tests. Load-strain diagrams of the first four circular concrete-filled tubes sections are presented below:

---

[3] Corresponding to the squash load of the composite section.
[4] See Section 4.4.1.1

Fig. V.1 Load-strain diagrams obtained for specimen 3MN.
Curves obtained in this investigation [left side]; curves used by (Susanta, et al., 2000) [right side].

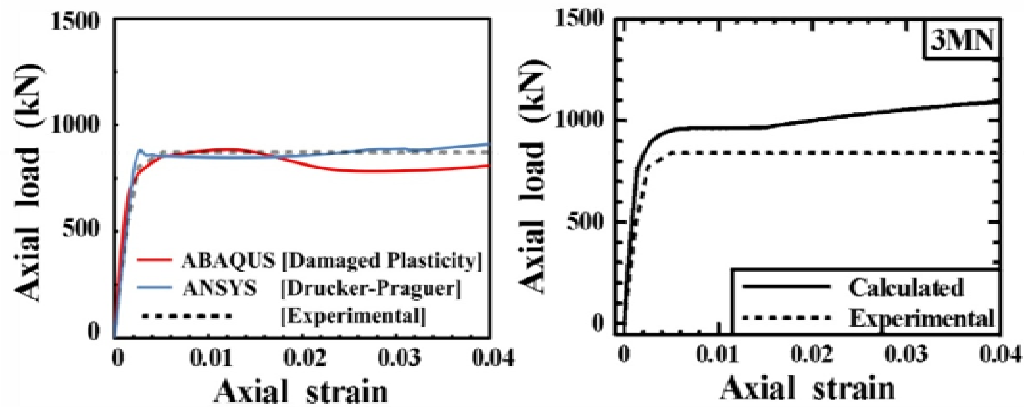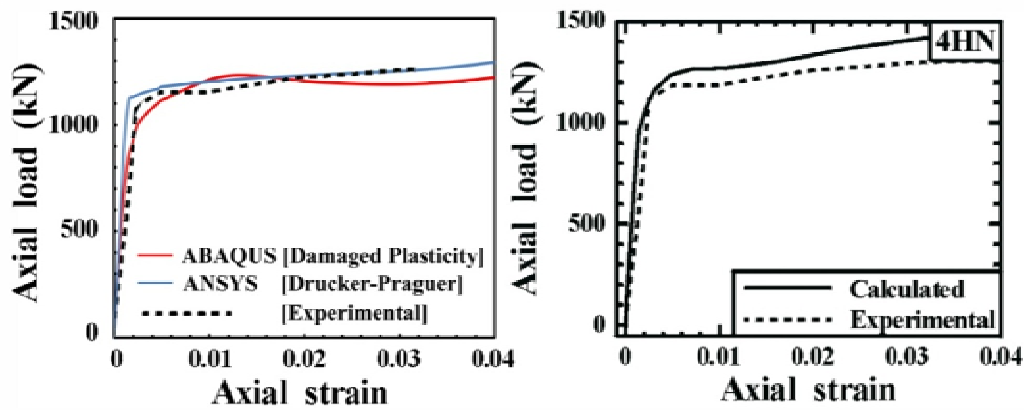**Fig. V.2 Load-strain diagrams obtained for specimen 4HN.**
Curves obtained in this investigation [left side]; curves used by (Susanta, et al., 2000) [right side].

Fig. V.3 Load-strain diagrams obtained for specimen CC4-C-4.
Curves obtained in this investigation [left side]; curves used by (Susanta, et al., 2000) [right side].
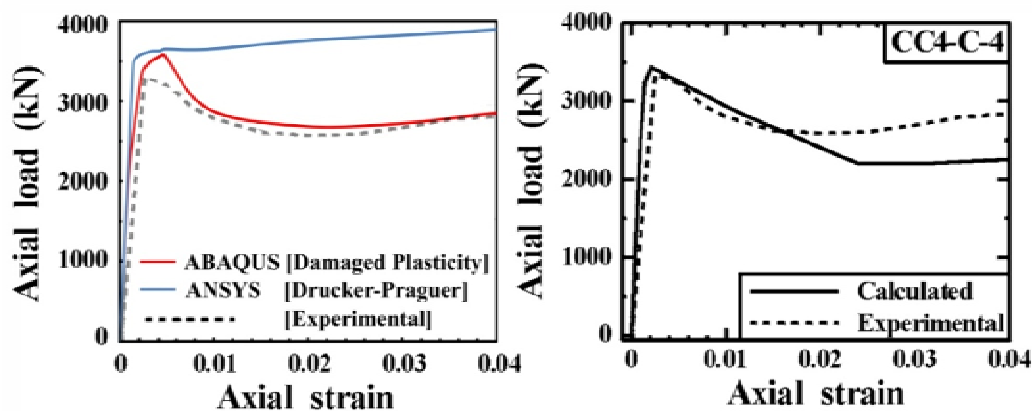
Fig. V.4 Load-strain diagrams obtained for specimen CF4-CC40.
Curves obtained in this investigation [left side]; curves used by (Susanta, et al., 2000) [right side].

As in case of circular concrete-filled tubes, the verification of the FE model has been done also for square-shaped sections, by using the same geometrical and constitutive resources. Few differences can be observed derived from the shape of the tube, apparently. Although the confinement effect on concrete core is normally lower in square-shaped CFT sections than in circular tubes, the descending branch during the softening period behaves really similar in both cases. Calibration curves for square-shaped sections are presented in the diagrams below:

Fig. V.5 Load-strain diagrams obtained for specimen S5.
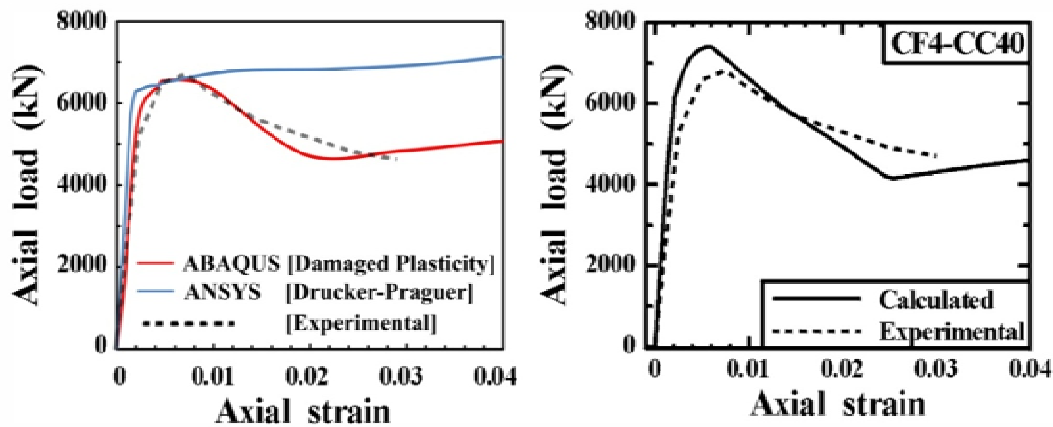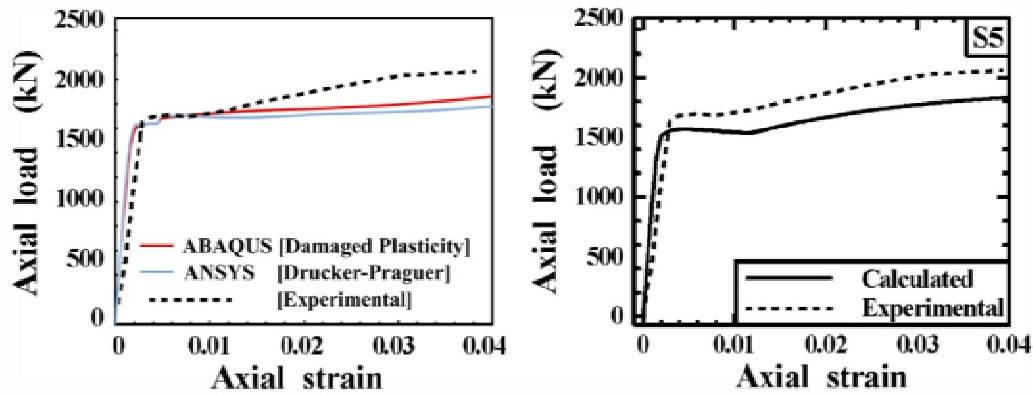Curves obtained in this investigation [left side]; curves used by (Susanta, et al., 2000) [right side].

Fig. V.6 Load-strain diagrams obtained for specimen S3.
Curves obtained in this investigation [left side]; curves used by (Susanta, et al., 2000) [right side].

Fig. V.7 Load-strain diagrams obtained for specimen CR4-A-4.
Curves obtained in this investigation [left side]; curves used by (Susanta, et al., 2000) [right side].

Fig. V.8 Load-strain diagrams obtained for specimen 4MN.
Curves obtained in this investigation [left side]; curves used by (Susanta, et al., 2000) [right side].
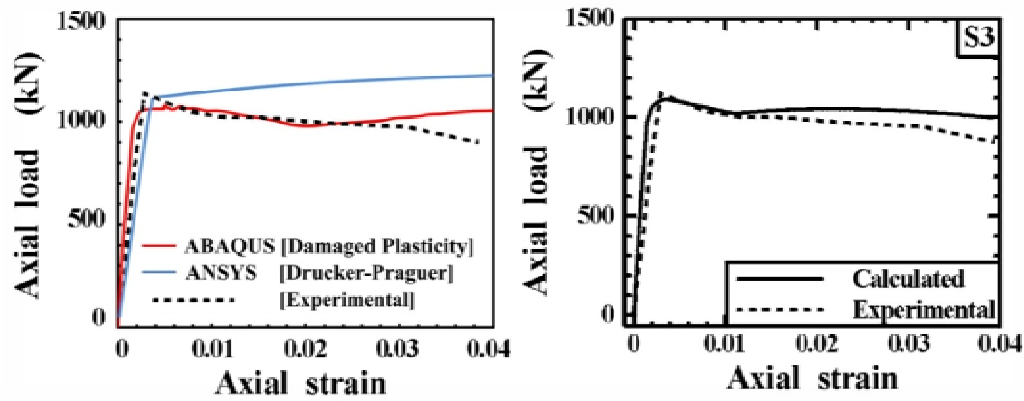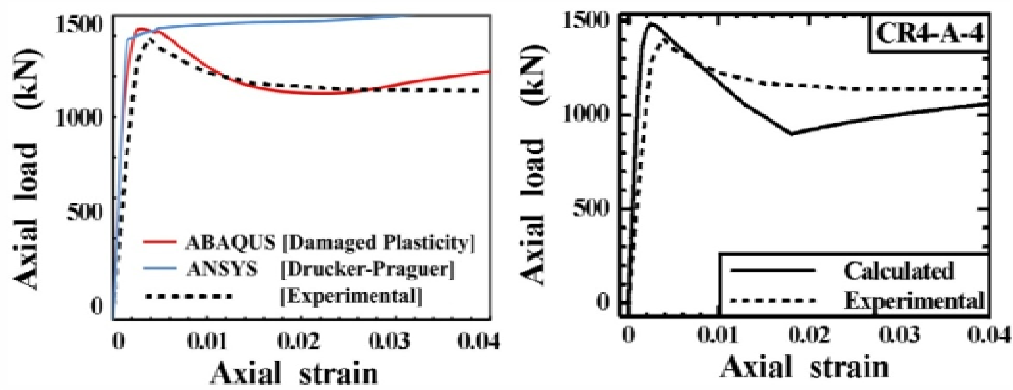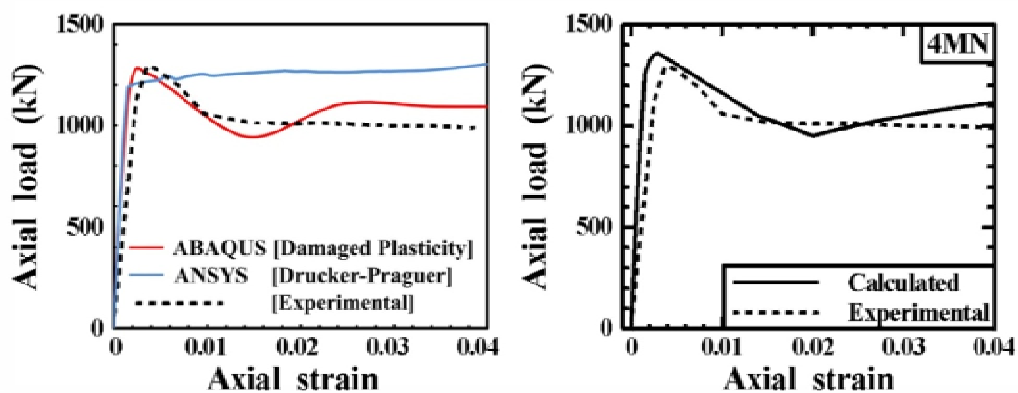
It is important to note how all the blue curves [those corresponding to an elastic-perfectly plastic model, based on the Drucker-Praguer yield criteria] do not show softening after the peak of load. Once the steel tube yields, plasticity of both materials is assumed infinite and the collapse does not occur. Contrarily, the red curves describe the relaxation of concrete after the *peak of load*, capable of reproducing the internal damage of the cohesive material.

5.2.2 Calibration of large deformation axial loading behavior.

Apart from calibrating the value of the maximum compressive load and also the post-peak behavior, it is also necessary to validate the obtained curves beyond deformations of 5%. To carry out this analysis up to these advanced percentages of deformation, the engineering stress-strain curve for steel is not valid, being necessary the use of the true stress-strain curve instead[5]. The axial behavior of CFT sections between strains of 10 and 20% is clearly sensitive to the hardening curve defined for steel, and also to geometrical nonlinearities of the plates.

In case of thick-walled CFT sections, local buckling does not appear in the elastic range; however it appears again at advanced plastic strains, really close to the collapse. As it has been explained in Section 4.5.1, a correct definition of the mesh size of the model is crucial to determine the mode of failure and buckling of the plates. A coarse mesh size could lead to important distortions of the plates and, therefore, to possible wrong results. At the same time, the definition of the stress-strain curve for steel by using the apparent values instead of the true values could involve an excessive dose of optimism in the prediction of the effects of hardening.

To ensure a good agreement between the results coming from the FE model and the curves coming from the experimental tests under large deformation axial loading [up to 25%], a CFDST section[6] has been used, coming from the investigation carried out by Zhao, Tong and others (Zhao, et al., 2010). General properties of the specimen are the following:

Table V.3. Geometrical and material features of specimen O6I2.

Section	D$_{out}$*	t$_{out}$*	D$_{inn}$*	t$_{inn}$*	fc**	fy**	L*	D/t
O6I2	165.10	3.00	101.60	3.20	63.4	395.0	500	55.03

All values expressed in mm* and N/mm^2**

As in case of circular and square-shaped CFT sections, the nomenclature of the specimen has been kept like the original, proposed by the author of this investigation. This experimental campaign was carried out by (Zhao, et al., 2010).

The sequence of the deformed shape coming from the finite element analysis is the following:

---

[5] See Section 4.4.1.1
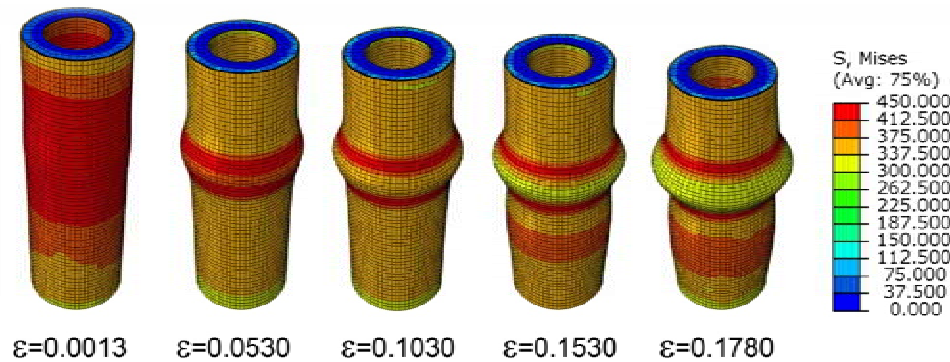[6] Concrete Filled Double Skin Tube

Fig. V.9 Sequence of large axial loading for specimen O6I2.
Deformed shape combined with von Mises stresses.

Full coincidence between the curve obtained from the analysis [in red] and the experimental [in black], obtained by Zhao (Zhao, et al., 2010), can be observed in the diagram shown below. The same boundary conditions and material strengths as those of the experiment have been reproduced in the simulation. The post-peak diagram fully matches with the experimental curve, and also the enhancement of strength corresponding to the hardening period is perfectly reproduced; only a slight delay is detected in the appearance of hardening effects in the load-strain curve.
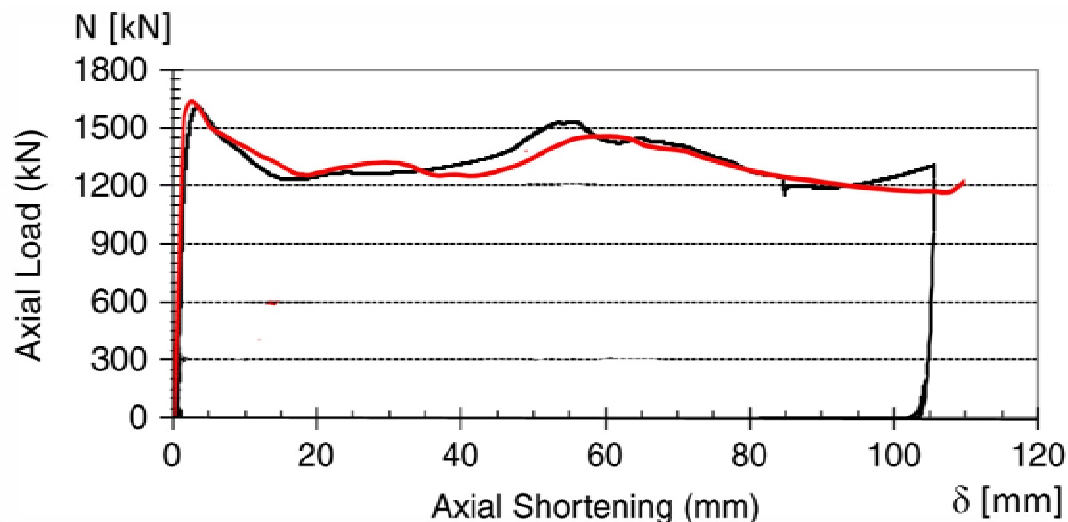

Fig. V.10 Calibration of large deformation axial loading model.
FEM analysis results [in red] and experimental results [in black] (Zhao, et al., 2010)

5.3 Description of compressive behavior of circular concrete-filled tubes.

Once the FE model has been calibrated from different points of view, the next two Sections pretend to use this calibration to describe the compressive behavior of CFT sections. For that purpose, two representative specimens from Tables V.1 and V.2 have been chosen and deeply analyzed: CF4-CC40 for circular-shaped sections, and CR4-A-2 for square-shaped tubes.

To get the final conclusions of this investigation, it is necessary to analyze and describe the behavior of components in CFT sections [steel and concrete] firstly, and to describe also the interaction between them, later. The analysis presented below belongs to one specific sample only, but it is intended that it can be generalized to most thick-walled sections.

5.3.1 Description of the complete axial load-strain diagram.

It is obvious that each specimen will have a different response under compression, even being all thick-walled CFT sections. The compressive behavior depends basically on the geometric [D/t] ratio and on the [f_y/f_c] proportion, between the two different material strengths. Differences in behavior are represented by the confinement effect on concrete filling, the percentage of damaged stiffness after the *peak of load* and the ductility and mode of failure at advanced stages of deformation.

All these phenomena are variable, depending on the mechanical properties of the two components. However, some common periods can be detected in the general load-strain diagram of CFT sections, circular-shaped in particular. General view of the sequence of the deformed shape until the collapse is shown in figure V.11:
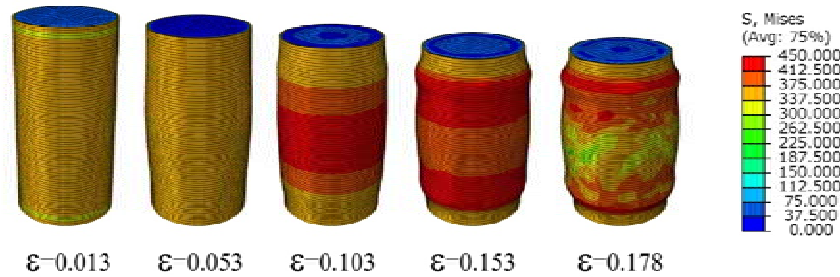

Fig. V.11 Sequence of loading of specimen CF4-CC40
Deformed shape of the loading process, superimposed with von Mises stresses.

Common periods detected in the load-strain diagram are the following: the elastic-plastic period [1], the softening period [2], the plastic hardening period [3] and finally, the collapse [4]. In the first short phase, the section reaches its maximum compressive strength and the confinement effect fully activates the core; after this point, as concrete filling is completely loaded, it starts a softening descent, depending on the compressive strength. During this period, the concrete of the core becomes mostly damaged by *crushing*. Beyond this point, an extended yield plateau takes place, during what the steel starts the hardening period at strains of 5%, up to the final collapse at about deformations between 0.15 and 0.18 [see figure V.12].

The important descending slope after the collapse is mainly due to the consideration of a symmetrical true stress-strain diagram for steel under tension, completely equivalent to that defined for compression [see Section 4.4.1.2]. Thus, the post-collapse behavior described by the curve of figure V.12 would be slightly smoother, owing to the appearance of tensile stresses in specific areas of the tube after the failure of the steel.
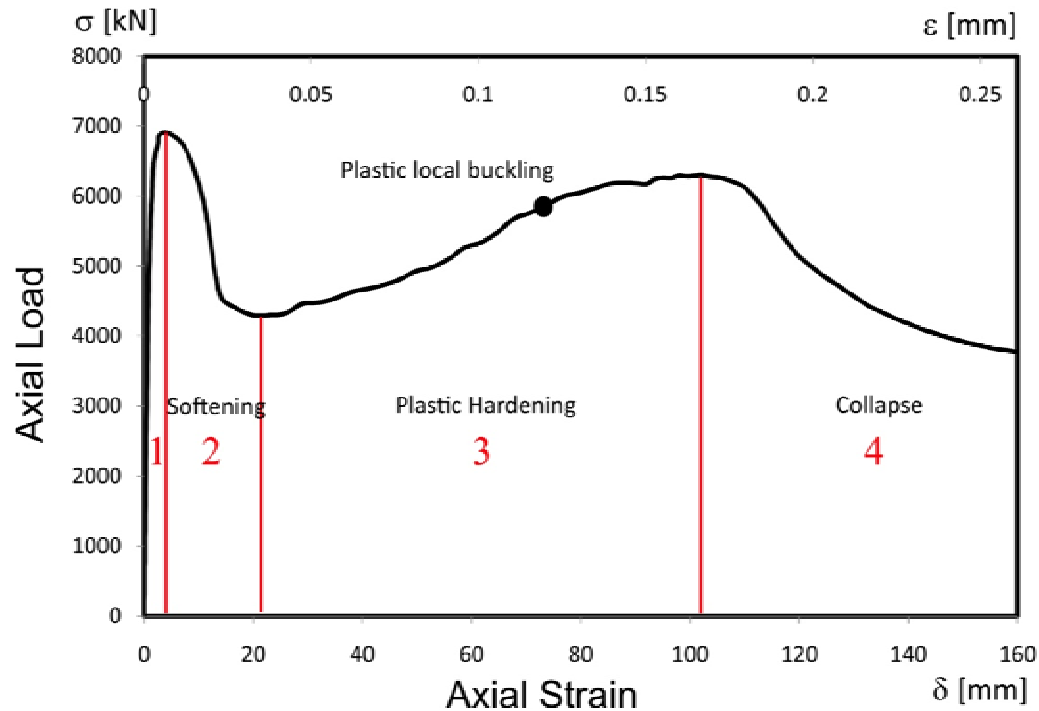
Fig. V.12 General Load-Strain obtained diagram of specimen CF4-CC40.
The four main periods can be clearly observed.

5.3.2 Description of the softening branch of the analyzed specimens.

As it has been commented before, the percentage of damaged concrete of the core depends basically on the ratio between the diameter and the thickness of the tube, as well as the proportion between material strengths of concrete and steel. The four different specimens which have been previously analyzed have been all compared in the diagram shown below for deformations until the percentage of 4%.

First of all, it is evident that sections filled with high strength concretes [between 40 and 50 MPa] show a sharper descent after the peak of load than those sections filled with concretes such as C20 or C30. Plastic vertical stress of high strength concretes during the hardening period decreases sharply, while in standard concretes [ranging from 20 to 30 MPa] this plastic descent is really smoother. This fact tends to delay the damage evolutionary process of the compressed concrete in those sections filled with concretes of the second group.

In conclusion, those sections which are more rigid [with low D/t ratios] and with low strength concretes do not show significant softening periods after the peak of load. On the contrary, those sections which are clearly less rigid or filled with high strength concrete do show important softening branches.
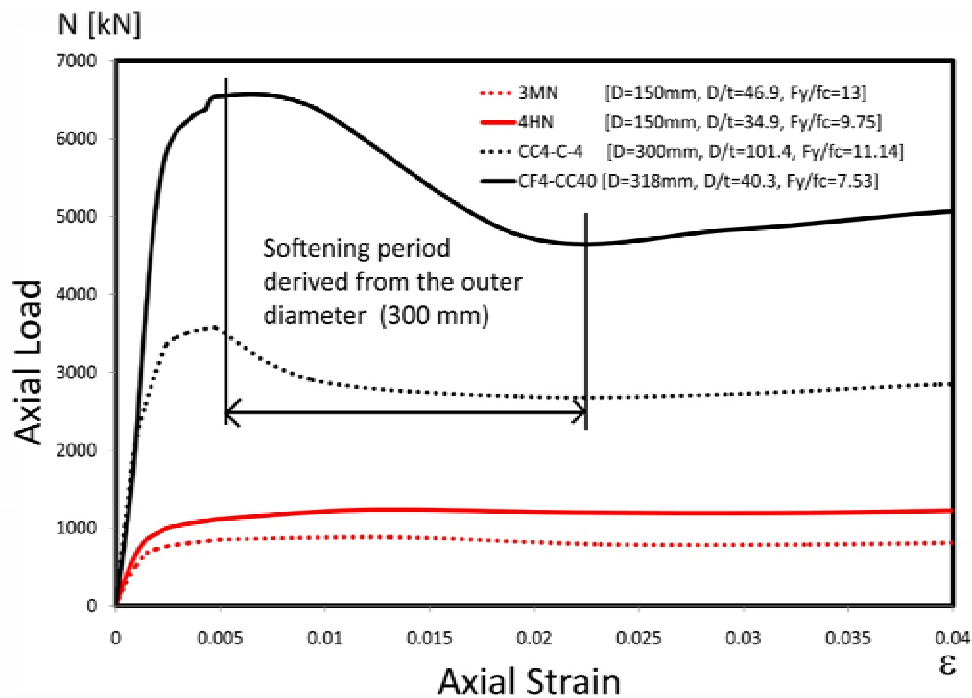
Fig. V.13 Comparison of load-strain diagrams between different circular CFT sections.
The two specimens in black have a diameter of 300 mm, while the two specimens in red have a
diameter of 150 mm.

5.3.3 Description of behavior of components in the loading process.

In circular-shaped concrete-filled tubes, the behavior of steel is decisive on the structural response of the composite section. In order to well understand the process of confinement effect on the core, the evolution of vertical and circumferential stresses of the steel tube has been analyzed, according to a cylindrical coordinate system.

The loading process in a circular CFT section until reaching the value of its *squash load* and beyond can be clearly understood through a detailed study of the evolution of axial and hoop stresses in the tube. The interaction between components [steel and concrete] is decisive in order to guarantee the load transferences during the process. From the analysis of the two principal stresses of steel [figure V.14], different load transferences between the tube and the core can be observed. In the first period (1) [elastic period], the steel tube absorbs most part of the load and no contact pressure exists between the two components, owing to the difference in the value of the Poisson's ratio: while the steel expands laterally more according to the value of its Poisson's ratio [0.289], concrete of the core expands by following a value of 0.18.

In this initial period, the core is subjected to a slight tensile hoop stress outwards -coming from lateral expansion of the tube and chemical adherence of the interface- combined with vertical compressive stress, derived from axial loading. On the contrary, steel is subjected to a biaxial compressive state [almost uniaxial, owing to the proportion between the components]. In case of exceeding the maximum value of adherence between the two surfaces, the contact tends to disappear and the two components start deforming clearly separately. Depending on this physical adherence, hoop stress of the tube is zero in this period [see Figure V.14], or negative instead. Physical adherence of the interface has not been considered in this investigation, according to the

existing literature, as it can be noted in figure V.14 [the value of the hoop stress during the first period is clearly zero, owing to the lack of contact].

In the second interval (2) [elastic confinement], concrete starts expanding laterally more than steel, owing to the level of its vertical stress; then, contact pressure between the two components takes place again. At this stage, the *apparent* Poisson's ratio of concrete is higher than that of steel[7], being this the unique reason why the core is confined by the tube. Beyond this point, the steel changes the uniaxial stress state by a biaxial state: both vertical and circumferential stresses of steel grow steadily during this period, owing to the increment of external load and thanks to the internal pressure derived from volumetric expansion of concrete.
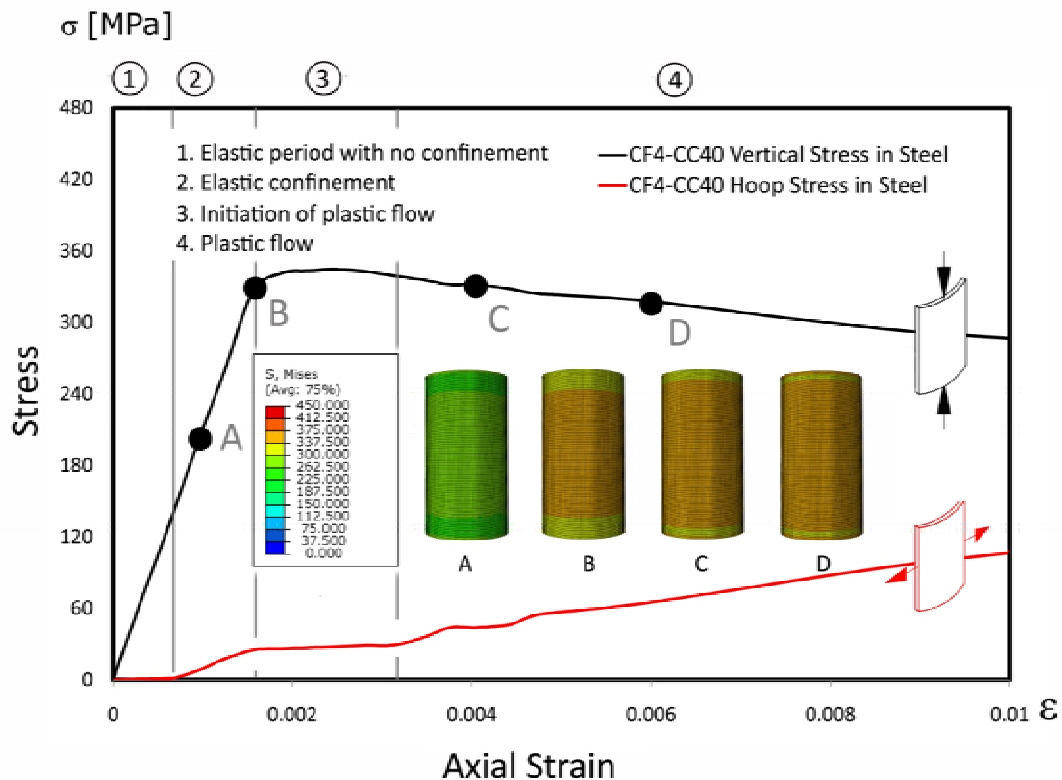

Fig. V.14 Detailed stress-strain diagram of the steel tube.
Vertical stress [in black], and hoop stress [in red] of specimen CF4-CC40, expressed in MPa.

During this second period, the first load transference from the steel tube to the core takes place; the increment of the hoop stress of the tube is converted into a uniform pressure on concrete core. Then, as concrete is subjected to a triaxial stress state, it becomes severely confined so that its compressive strength is clearly enhanced according to the postulates of Richart (Richart, et al., 1928). The reduction of the vertical strength of the tube and the progressive enhancement of the compressive capacity of concrete contribute to generate a first load transference from the first to the latter in zone 2. This second period finishes when the steel of the tube finally yields.

When the combined von Mises stress of the tube reaches its maximum yield limit value, the two components of stress [vertical and circumferential] stop growing up, and start flowing. This third period is numbered separately in Figure V.14 as phase (3) [initiation of plastic flow]. From this initial flow of steel, where neither the hoop stress nor the vertical stress do not change significantly, the flow rule is superimposed to the stress state and the material starts yielding by following the

---

[7] The *apparent Poisson's ratio* of concrete can be higher than its theoretical limit [0.50], as the material subjected to high stress levels tends to expand by crushing the cement paste between the aggregates.

elliptical curve of von Mises [phase (4), plastic flow]: this means that the vertical stress starts a clear descent, while the circumferential shows a clear growth instead.

This last period is characterized by a high increment of confinement effect on the concrete core.
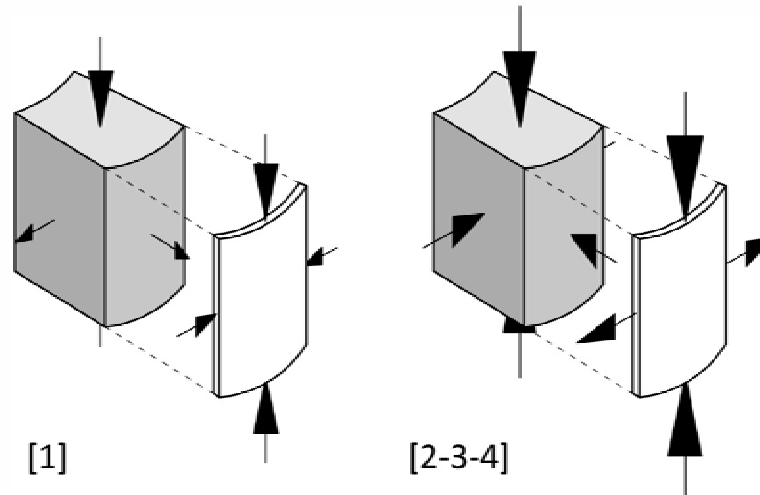

Fig. V.15 Stress states of the concrete core and the steel tube.
The numbering refers to the different mentioned periods of figure V.14.
Hoop compressive stress of period [1] is assumed zero in Fig. V.14, instead of negative.

As it is shown in figure V.15, during the first period [1], the concrete of the core is subjected to a slight triaxial stress state, since the tensile stress in the radial and circumferential directions is really small [supposed zero], due to the physical adherence between components. In the same way, steel of the tube is subjected to a biaxial compressive stress state. In the other three periods [2-3-4], concrete becomes clearly triaxially compressed, while the steel of the tube gets tensioned in the circumferential direction and compressed in the vertical direction.

It is really curious to see how vertical stress of the steel tube decreases from an approximate strain of 0.002, while vertical stress of concrete goes on growing until its maximum confined compressive strength, f_{cc} [see Fig. V.16]. Since the steel of the tube is already yielding [according to the von Mises yield criterion] vertical stress decreases in a similar proportion as that the hoop stress grows. This enhancement of the circumferential stress is directly converted into confining pressure on concrete core. In the phase of the curve between points B and D, the load transference takes place from the tube to the core.

The first period colored in red corresponds to the phase during which concrete behaves almost elastic, performing completely separately of steel owing to the explicit difference in their elastic Poisson's ratios. From an approximate vertical stress of 120 MPa, reached by the steel tube, concrete starts to expand laterally more than the theoretical deformation predicted by the value of its Poisson's ratio.
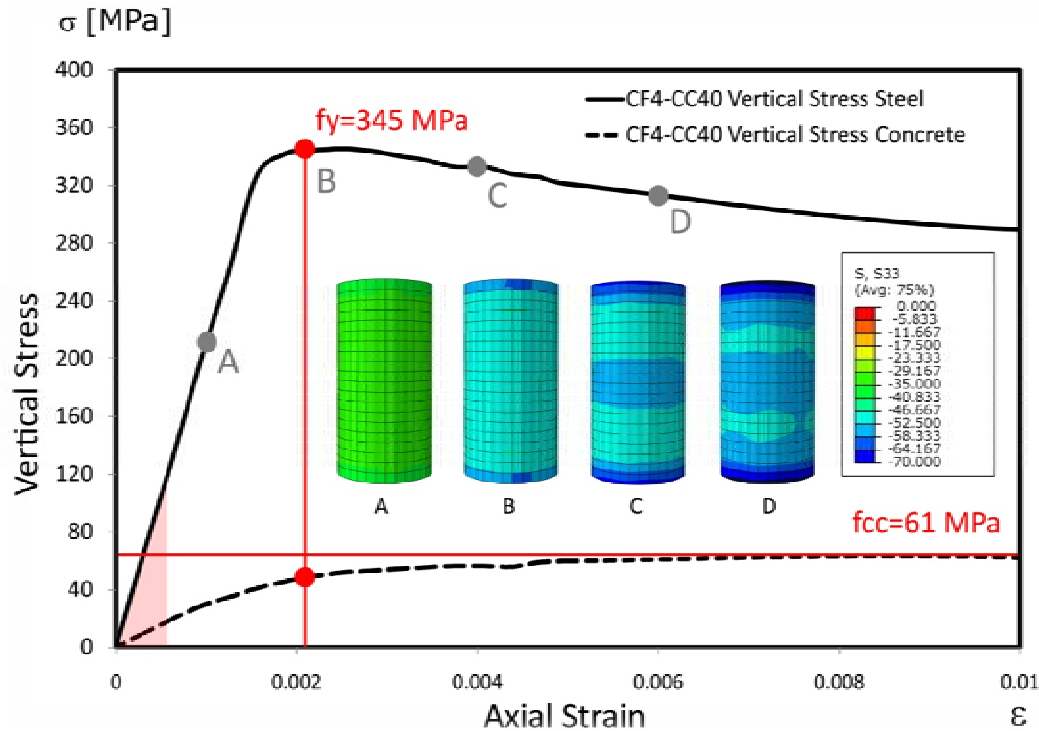
Fig. V.16 Comparison between vertical stresses obtained for steel and concrete.
Evolutionary sequence of vertical stress in steel [continuous line],
and vertical stress of concrete core [dashed line], expressed in MPa.

It is important to observe that most part of the growth of concrete strength owing to confinement occurs from point B in figure V.16. This point determines the initiation of yielding of the steel tube; according to the flow rule, steel must flow by following the von Mises elliptical curve, by combining vertical and hoop stresses. In case of flowing to the left side of the elliptical curve, vertical stress grows, while circumferential stress diminishes; otherwise, the first one is reduced while the latter is enhanced. This last assumption is the one which fully matches with the real behavior [as it can be observed in figure V.19].

Hoop stress of the steel tube is quickly converted into confinement on concrete core, growing concentrically from the centroid to the perimeter [as it can be seen in the sequence presented in figure V.17]. Concrete under these conditions improves considerably its compressive strength, enhancing also the load-bearing capacity of the composite section.
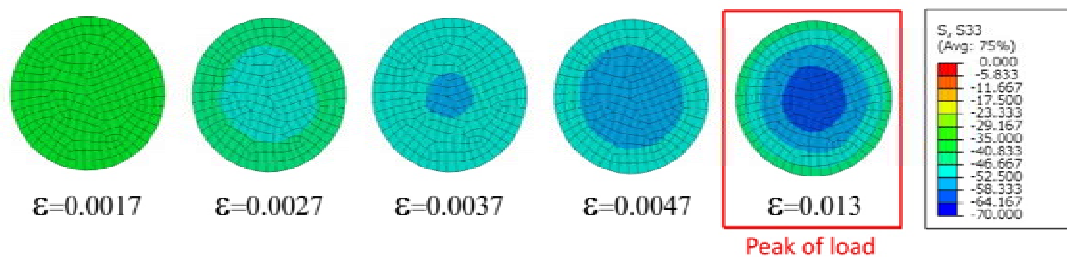

Fig. V.17 Evolutionary sequence of vertical stress in concrete core, until the peak of load.
The evolution of confinement effect on the core can be clearly observed, expressed in MPa.

Beyond point D of the stress-strain curve in figure V.16, and after the softening period of concrete, a wide yield plateau takes place. The descending branch after the *peak of load* depends basically on the thickness of the outer tube and the mechanical properties of the concrete filling[8]. After the plastic flow there is a second ascending period caused by the hardening effect, and characteristic of steel [from point E to point F in figure V.18], where vertical stresses grow up to 25-30% more. At strains approximately of 10-12%, local buckling effects are observed in the plastic range, located in the nearby of the embedded faces.
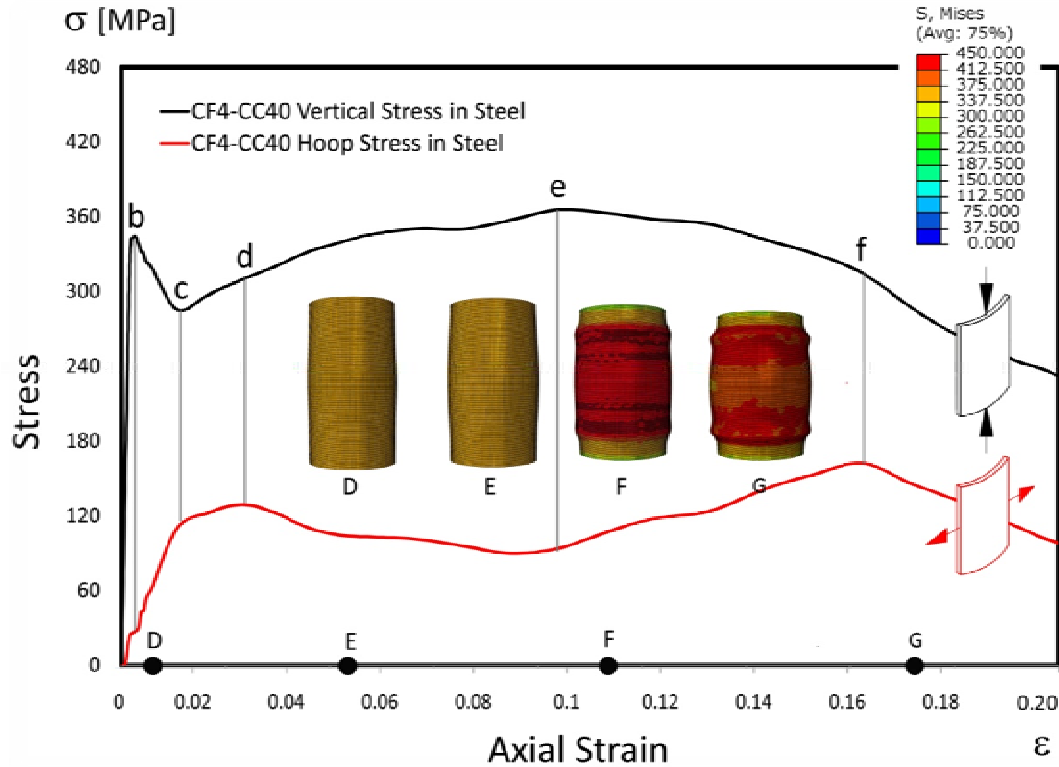

Fig. V.18 Averaged stress-strain diagrams of the steel tube, obtained from the FE analysis.
Vertical stress [in black] and hoop stress [in red], expressed in MPa.

The appearance of local buckling effects in advanced deformation ratios leads to an important descent of vertical stress of the steel tube, until the collapse of the global section. It is curious to see how vertical stress of steel decreases from point F to point G, while the circumferential stress is still growing up. This is the reason why confinement effect goes on growing to the collapse and why the maximum compressive strength of the concrete filling reaches its maximum value after the peak of load, at the extraordinary values of strain of 0.14-0.15. However, although concrete at this point has a load-bearing capacity well above its maximum uniaxial compressive strength [see figure V.21], the material at this point is already damaged, as a consequence of the process of crushing.

The evolution of the stress components in the steel tube is so decisive and so complex at the same time that it is really interesting to represent the loading path in the biaxial stress plane, where the ordinates coincide with vertical stress, and the abscissas with hoop stress[9]. The same points **a, b, c, d, e** and **f** can be detected in this diagram, and full coincidence with the von Mises yield criterion is observed after the yield limit stress [zone **b-c**]. As it has been commented before, after yielding,

---

[8] as it has been explained in Section 5.3.2
[9] Both components have been considered positive, although σ_1 refers to compression.

steel flows to the right direction by following the elliptical curve of von Mises; this fact leads to an increment of hoop stress and to a decrement of vertical stress in the tube, although the global compressive response of the section is still being improved. The erratic trajectory from point **c** to **e** corresponds to the expansion of the von Mises yield surface owing to the hardening period, in the isotropic hardening model used for steel.
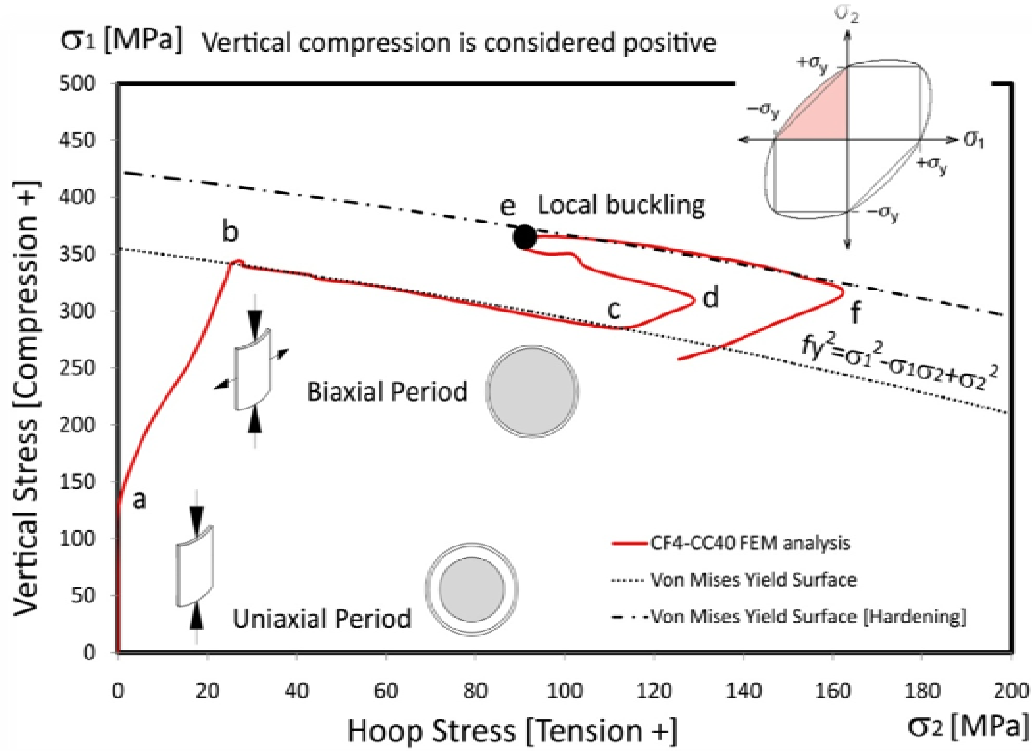

Fig. V.19 Loading path of steel in the biaxial stress plane.
Full coincidence with the von Mises elliptical curve is observed, expressed in MPa.

In figure V.20, the correspondence between vertical and circumferential stresses of concrete in the nearby of the peak of load [point D] is shown. In order to corroborate the results obtained from the FE analysis again, the postulate of Richart (Richart, et al., 1928) has been used to determine the validity of the value of circumferential stress [about 4 MPa]. According to the expression:

$$f_{cc} = f_c + m \cdot \sigma_r \qquad (2.19)$$

and knowing that f_{cc} = 61 MPa , f_c = 47.5 MPa and m = 4.1 , [Fig. V.16] we can calculate:

$$\sigma_r = 3.37 \text{ MPa} \qquad (5.2)$$

This value is really close to those obtained from the diagram. Furthermore, and according to the investigation carried out by Susantha and Ge (Susanta, et al., 2000), the relation existing between the circumferential stress of concrete and the hoop stress of steel can be easily obtained through:

$$\sigma_{\text{hoop,a}} = \left[\frac{D - 2 \cdot t}{2 \cdot t} \right] \cdot \sigma_r = 19.23 \qquad (5.3)$$

Then, by using the value of the hoop stress for steel, we can obtain the following value for the maximum confined strength of concrete:

$$f_{cc} = 64.80 \, \text{MPa} \qquad\qquad \textbf{\textit{(5.4)}}$$

Both values (5.3) and (5.4) coincide with the values corresponding to the curves for hoop stress of steel in point D [figure V.18] and for vertical maximum stress of concrete [figure V.20]. The evolutionary curve of vertical stress of the concrete filling is represented in the following diagram:
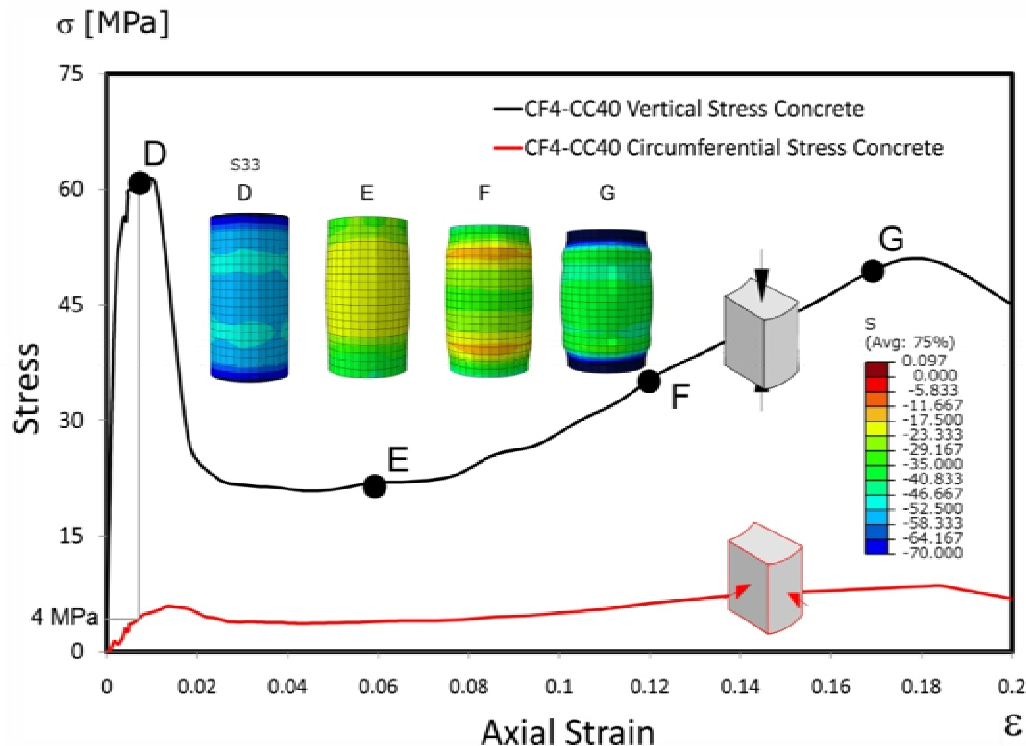

Fig. V.20 Stress-strain diagrams of the concrete core, obtained from the FE analysis.
Vertical stress [in black] and circumferential stress [in red], expressed in MPa.

The evolution of the stress state beyond the peak of load is represented in the following sequence, where an important decrease in strength can be observed coinciding with the softening period. A surprising load-bearing capacity of the core at advanced strains of 15 and 18% can be also detected. This phenomenon is due to the hardening period of steel, since concrete behavior at this point is more similar to a filling of sand than to a cohesive material, as most part of the cement paste is already crushed[10]. Under this state, concrete resists much part of the load thanks to be contained in the tube, and this fact improves the global ductility of the section.
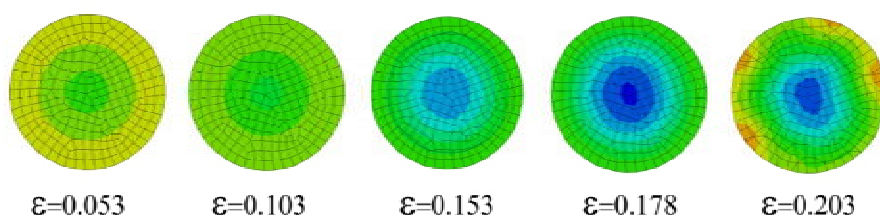

$\varepsilon=0.053$ $\qquad$ $\varepsilon=0.103$ $\qquad$ $\varepsilon=0.153$ $\qquad$ $\varepsilon=0.178$ $\qquad$ $\varepsilon=0.203$

Fig. V.21 Evolutionary sequence of vertical stress in concrete core, after the peak of load.
It can be seen how the maximum confined strength is reached at strains of 0.17.

---

[10] See Section 5.3.4

195

5.3.4 Evolutionary compressive damage description of concrete core.

To do a complete analysis of large deformation axial loading of CFT sections, it is necessary to supplement the tensional lecture with a damage evolutionary analysis of the concrete filling. Concrete, as a cohesive material formed by the cement paste and the aggregates, suffers from progressive stiffness degradation when it is subjected to high levels of stress. This degradation is clearly different under tension [*cracking*] than under compression [*crushing*], as it has been explained in Chapter IV. As it can be derived from the sequence presented below, [see Fig. V.22], at the peak of load, concrete of the core is already damaged in a 15-20%. This means that axial stiffness of the material would be reduced in a 20% in case of being reloaded, [see Chapter IV].

Beyond the peak of load, the evolution of the compressive damage ratio in concrete core is really fast, due to the advanced deformation rates. At strains between 5% and 8%, the whole concrete filling is already damaged over the 60%, and the composite section is not longer suitable for structural purposes [although it could still resist high loading levels]. The evolution of the compressive damage ratio is represented by the scalar coefficient, d_c, ranging from 0 to 1:
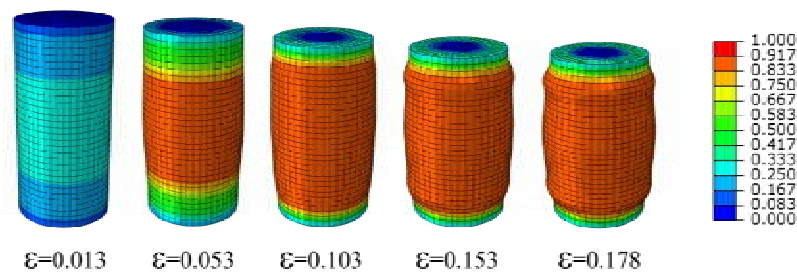

Fig. V.22 Evolutionary compressive damage ratio in concrete core.
From strains of 5%, the whole concrete core is damaged in the 60% in average.

In figure V.23, the evolution of vertical stress is compared with the evolution of compressive damage in the core. Note how damage goes always further, while vertical stress decreases during the softening period and grows during the hardening phase. It is really surprising to discover that, although concrete resists high levels of stress at incredible axial displacements of 80-100mm, the material is completely damaged in a 80% at these points. Besides, this evolutionary damage process is characterized for being irreversible.

Note how important the softening period is on determining the evolution of the damage process; main part of the damage occurs just between the peak of load and the yield plateau. This means that a significant restrain of the softening behavior after the peak of load leads to delay the damage evolutionary process: this will be more accurately described in further Chapters.
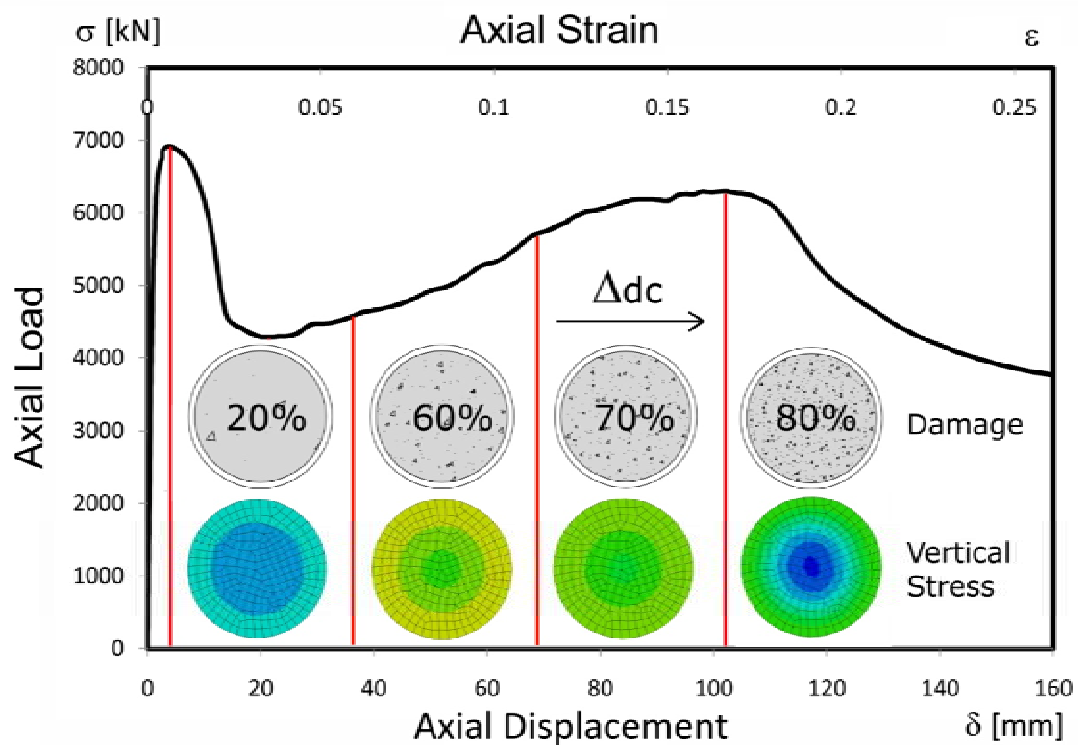
Fig. V.23 Evolutionary compressive damage ratio of concrete core.
No correspondence is observed between the evolution of damage and the evolution of vertical stresses in concrete core.

5.3.5 Description of ductility and mode of failure.

Ductility is one of the most representative mechanical qualities of CFT sections, especially in case of circular-shaped tubes. The well-known ductility of steel improves the axial response of concrete of the core considerably, although the latter is already completely damaged at advanced percentages of strain. Ductility is decisive in seismic designs, where the priority is to be capable of absorbing the more energy as possible, by guaranteeing the global stability of the structure at the same time.

Final collapse of circular CFT sections takes place at strains about 15-17%, [depending on material strengths and tube thicknesses]. These values are really elevated, compared with other structural solutions. The mode of failure follows always the same pattern for thick-walled tube sections: firstly, the tube starts buckling according to the mode known as "*elephant foot*" before reaching the maximum hardening stress; secondly, when the steel tube has been failed, the concrete collapses by following a plane of rupture at approximately 45° respect to the horizontal.

As it has been explained in Section 5.3.1, when the section reaches the peak of load, part of the load has been already transferred to the core; after this point, concrete starts to degrade progressively up to the initiation of the yield plateau and, close to deformations between 5 and 10%, the steel starts the hardening period where its strength is enhanced up to 30% more. During this period, the load is transferred again from the core to the tube, until the appearance of local buckling in the nearby of the loaded edges. The mode of buckling in these cases is the mentioned as "*elephant foot*", and it leads to the final and definitive load transference, from the tube to the core. An important load increment over the damaged concrete is clearly excessive at this advanced stages of loading,

and this leads also to a sharp collapse of the core. The concrete tends to fail through a plane of rupture at 45° respect to the horizontal, by following the condition of a cohesive material.
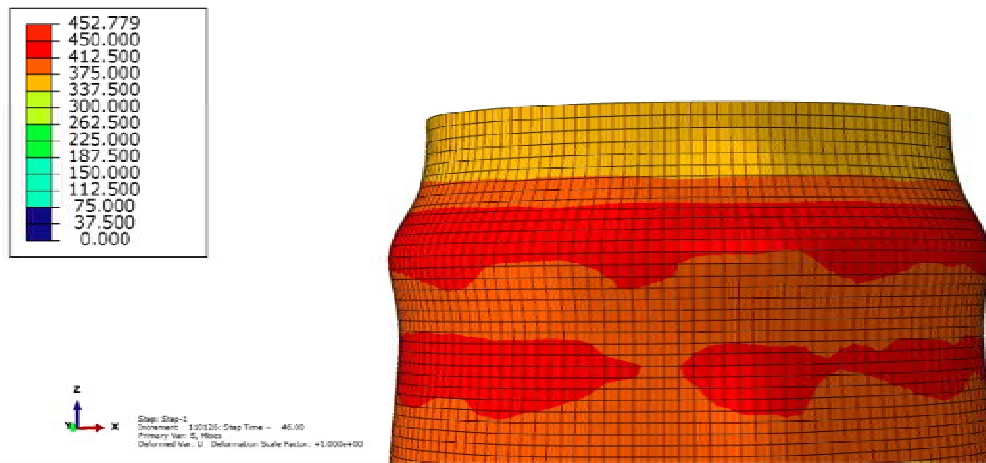

Fig. V.24 Local buckling of circular CFT sections in the plastic range.
The mode of buckling is known as "*Elephant foot*".

The appearance of local buckling in advanced plastic strains determines the beginning of the global collapse. For thin-walled concrete filled tubes, buckling occurs in the elastic range, and it follows the differential equations for cylindrical shells presented in Chapter III; on the contrary, for thick-walled tubes, buckling does not occur until advanced values of axial strain about 10%. The half wavelength of the shell is about 0.5 times the length of the undeformed diameter. Although the sections shown in figure V.25 have different geometries and also different material strengths, close similarities can be observed between results of an experimental test [carried out by Liew and Xiong (Liew, et al., 2009), on the left] and results coming from the FEM analysis carried out in this investigation:

Fig. V.25 Similarity between the mode of failure obtained in the FE analysis and the experimental tests carried out by (Liew, et al., 2009).

5.3.6 Evolutionary description of contact pressure between components.

Contact pressure on concrete talks about the confinement effect over the core, clearly. In figure V.26 it can be seen how uniform the contact pressure is on the concrete filling in circular CFT sections. Normal values are below 10 MPa at those stages close to the peak of load. This uniformity of lateral pressure is directly converted into efficiency of the confinement effect in circular CFT sections.
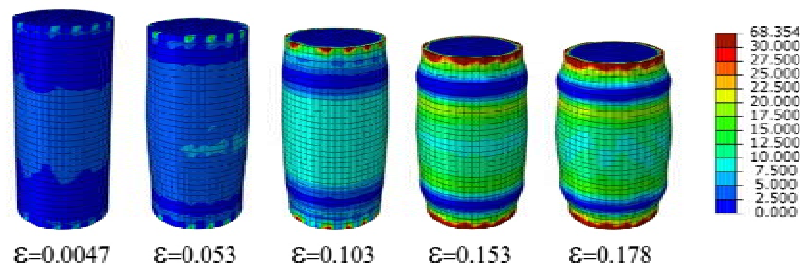

Fig. V.26 Evolution of contact pressure on concrete core, circular sections, expressed in MPa.
Note how uniform is the confinement effect on the core, owing to the uniformity of pressure.

See how contact pressure ranges from 4 to 7 MPa in the nearby of the peak of load [between first and second frame of Fig. V.26]; this value coincides with the circumferential stress of the core, shown in figure V.20. Thus, it is evident that the interaction between the two materials is decisive in order to reach the maximum compressive strength of the composite section, since it is the steel tube the one which applies the confining pressure over the core. As axial strain progresses, lateral pressure on central parts of the core is even enhanced coming from the extraordinary influence of volumetric expansion of concrete.

Needless to say that those areas coinciding with local buckling of the tube are progressively unloaded, even separating from steel [see the third and fourth frames of the sequence in figure V.26, which are clearly blue-colored].

5.4 Description of compressive behavior of square-shaped concrete-filled tubes.

To describe the behavior of square-shaped CFT sections, the specimen 4LN[11] from table V.2 has been chosen; it is intended that the compressive behavior of this section, square-shaped, and clearly thick-walled, can be generalized to other geometries and material strengths.

5.4.1 Description of the complete axial load-strain diagram.

Although the compressive behavior of square-shaped concrete-filled tubes is really similar to the behavior of those circular sections in general terms, there are some basic differences which have to be necessarily considered. The two most important differences in compressive behavior are: on the one hand, the clear reduction of the influence of confinement effect, and on the other hand, the significant decrement of ductility.
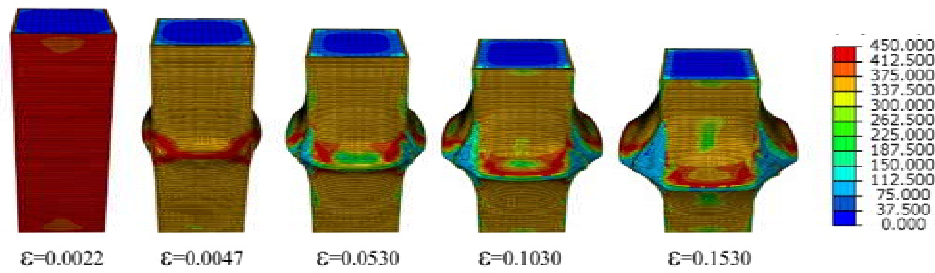
---

[11] Susantha and Ge (Susantha, et al., 2000)

Fig. V.27 Sequence of large deformation axial loading of specimen 4LN.
A high deformability of the plates implies an earlier collapse.

In the sequence which is shown before [Fig. V.27], it can be clearly seen how the failure of the specimen starts much earlier than in case of circular sections. Ductility in square-shaped tubes is lower compared to the ductility shown by circular sections, owing basically to geometrical reasons strictly: rectangular plates are flexed in double curvature by internal pressure coming from volumetric expansion of the core, while cylindrical shells are circumferentially tensioned thanks to the circular geometry. Since flexural stiffness of the plates is much lower than their axial rigidity, the collapse of square-shaped tubes normally occurs earlier than in circular-shaped tubes [see Fig. V.28].
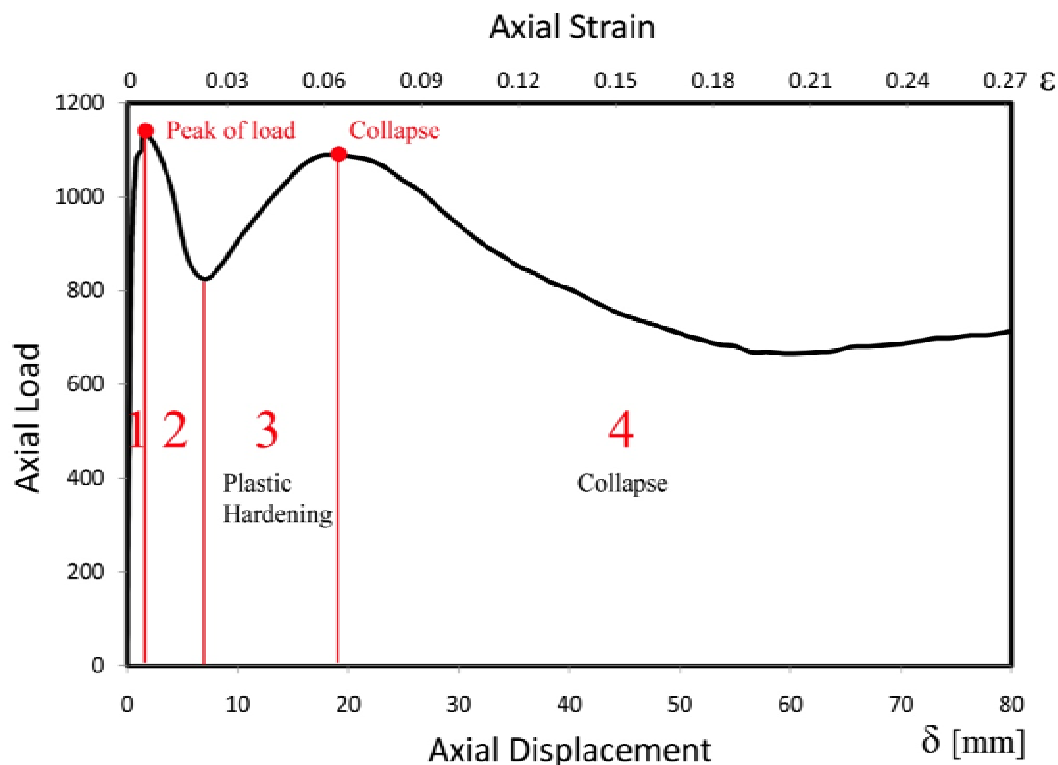

Fig. V.28 General Load-Strain diagram of specimen 4LN, obtained from the FE analysis.
The same four periods as in case of circular sections can be clearly observed.

Besides, it can be seen in diagram of figure V.28 that the plastic hardening period is also much shorter than in circular tubes, owing to the appearance of geometrical nonlinearities of the plates. The collapse occurs at approximate strains between 5 and 6%, clearly earlier stages of loading.

The post-collapse diagram shows a significant descent, mainly due to the use of a true stress-strain diagram for steel under compression only. Before the collapse, most part of the tube is compressed; under this assumption, the use of the true stress curve under compression [Fig. IV.17] gives a better approximation to the real response of steel than that provided by the true stress curve for tension. The implementation of the second curve would lead to overestimate the enhancement of steel during the hardening period, while the use of the latter responds accurately to reality before the collapse. However, the use of the first tends to accelerate the collapse as the strength under tension quickly decreases [see Section 5.4.3].

5.4.2 Description of the softening branch in the analyzed specimens.

As in case of circular CFT sections, square-shaped tubes with low B/t ratios do not show significant softening periods, behaving as almost elastic perfectly-plastic materials [see the horizontal curve of specimens S3 and S5]. On the contrary, rectangular tubes with higher B/t ratios usually show an important softening behavior after the peak of load, even more than circular concrete-filled tubes owing to the deformability of the plates.

The specimens analyzed in this investigation do not show important differences between them, in reference to the softening behavior. This is due to their reduced global size, and specially to their low B/t ratios.
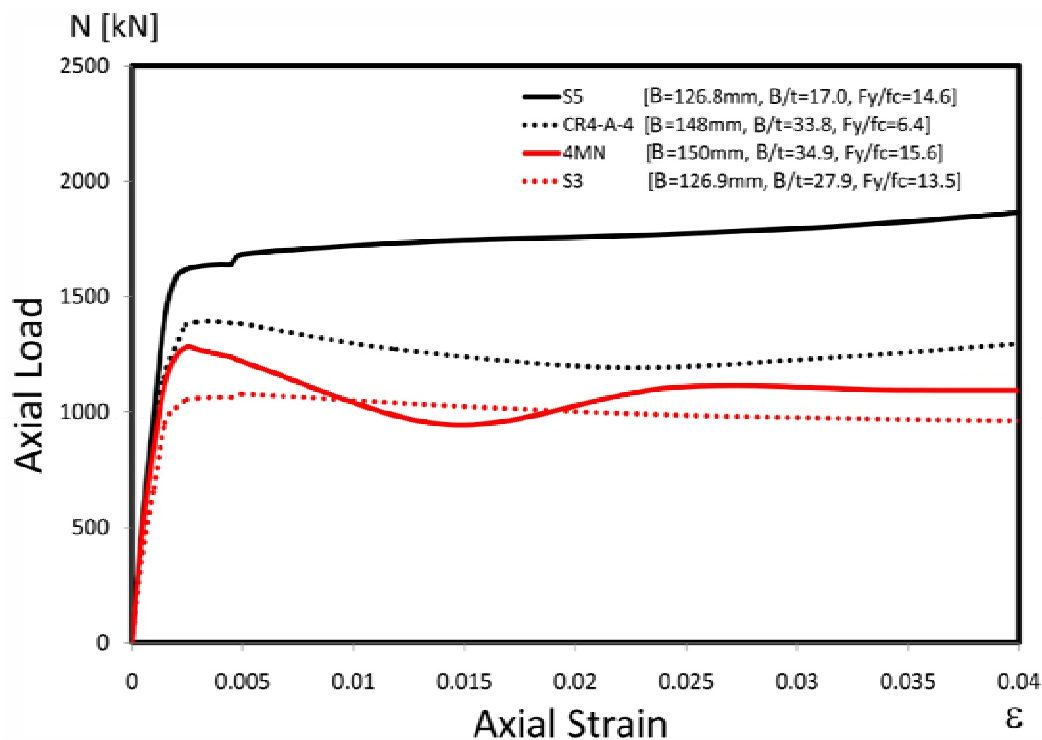

Fig. V.29 Different load-strain diagrams for the analyzed square-shaped sections.
These specimens do not show important softening behaviors after the peak of load, except for the case of section 4MN, due to the reduced size of the tube width.

5.4.3 Description of behavior of components in the loading process.

Although the behavior of components is relatively similar to that explained for circular specimens, there are some light differences associated with the value of the maximum squash load. The four periods mentioned in Section 5.3.3 for steel can be also detected in the stress-strain diagram of section 4LN. Confinement effect also appears in square-shaped sections, by following a slightly different pattern than that described by circular sections. The difference lies basically in the deformability of the plates: while vertical edges in square-shaped tubes are considered almost infinitely rigid, central areas of the plates show a low flexural rigidity.

While the stress distribution in circular tubes is uniform almost during the whole loading process, vertical stress in square-shaped tubes is notably lower in central areas of the sides than in the proximity of the edges. Owing to the difference of rigidity between the edges and the plates, most part of the distributed pressure coming from the dilatancy of the core is absorbed by the edges, through a compressive force in arch effect. Contrarily, the plates deform in their mid-span as a uniformly loaded slab, being not capable of confining the concrete core in these areas.

As it can be derived from point A of figure V.30, vertical stresses corresponding to central areas of the plates are really lower than vertical stresses of the edges. This phenomenon is clearly caused by the elevated rigidity of the edges. The tensional distribution in steel describes the pattern of confinement on concrete core: the existing difference between flexural rigidities originates a natural distribution of the compressive stress on the [yz] plane in arch effect, from one edge to other [see figure V.31]. Thus, those areas of the core corresponding with central parts of the plates are not affected by confinement effect.
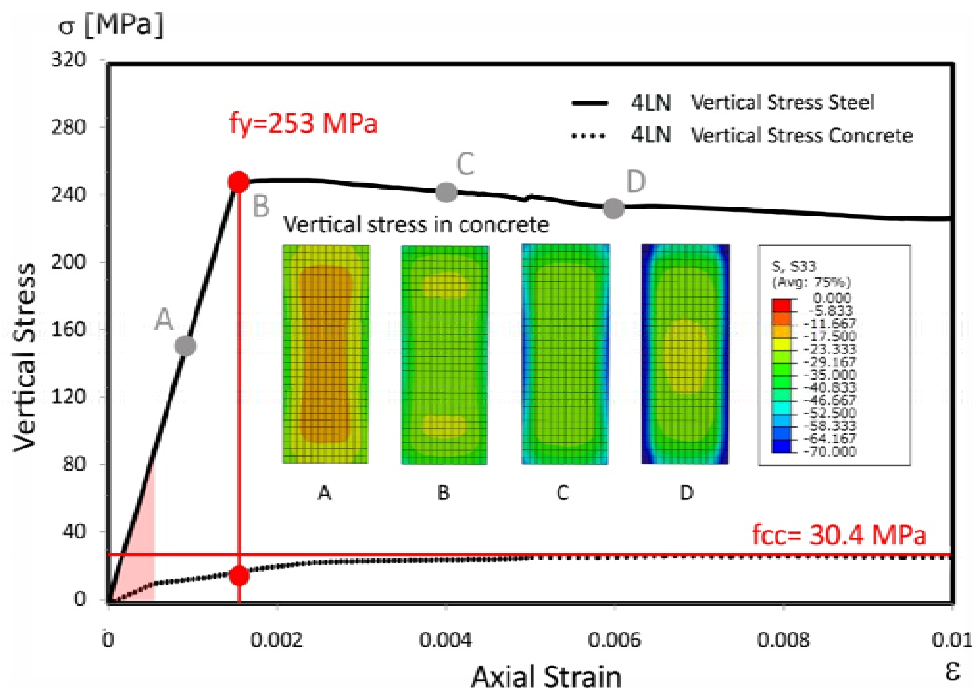

Fig. V.30 Comparison between the evolution of vertical stress in steel and concrete.
Curves obtained from the FE analysis for specimen 4LN, expressed in MPa.

From figure V.30, it can be seen how vertical stress in steel starts going down from point B, while concrete goes on increasing its strength. This effect was noted also in circular CFT sections, and it is basically due to the plastic flow of steel derived from the elliptical curve of von Mises. Assuming

that confinement effect of the core never reaches so high values as in a homologous circular section, the shape adopted by the triaxially compressed areas of the core can be idealized as it is shown in figure V.31 [according to (Chen, et al., 2006)]:
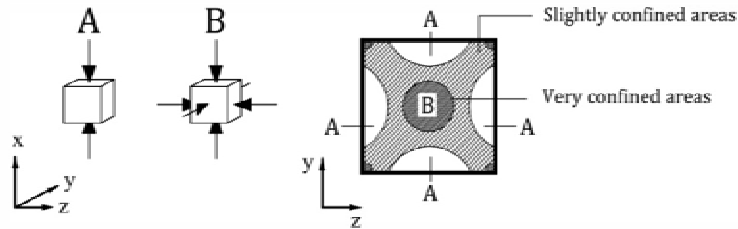

Fig. V.31 Idealized pattern of confinement in square-shaped CFT sections.
The shape of the confined area in arch effect from one edge to other can be clearly observed.
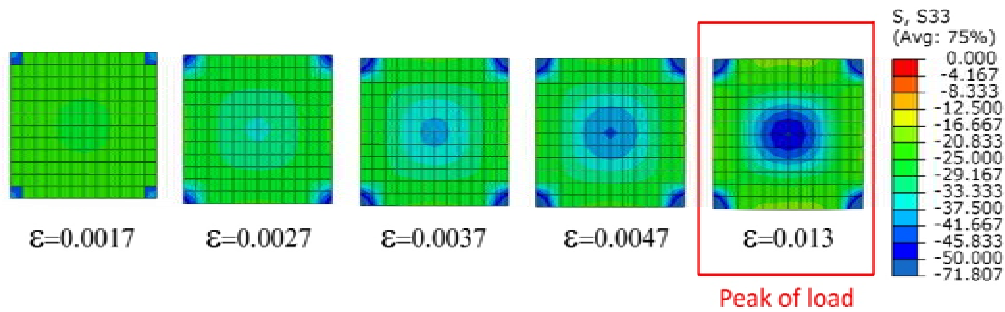

Fig. V.32 Evolution of vertical stress in concrete core, up to the peak of load [MPa].
Note how the confinement effect grows outwards, from the centroid to the perimeter.

The volumetric expansion of the core takes place concentrically from the centroid; as a consequence, and owing to the square-shaped geometry, significant bending moments appear in the mid-height of the plates. Wall-thickness of central parts of the plates goes from a pure compressive state to a combined flexural state, due to the difference in rigidity between these areas and the edges; this fact entails an important reduction of ductility of the global section, since axial stiffness of a plate is always higher than its flexural rigidity [see figure V.33]. While in circular sections the tube is subjected to a combination of vertical compression and circumferential tension, in square-shaped tubes the plates go from a pure compressive state to a flexural state.
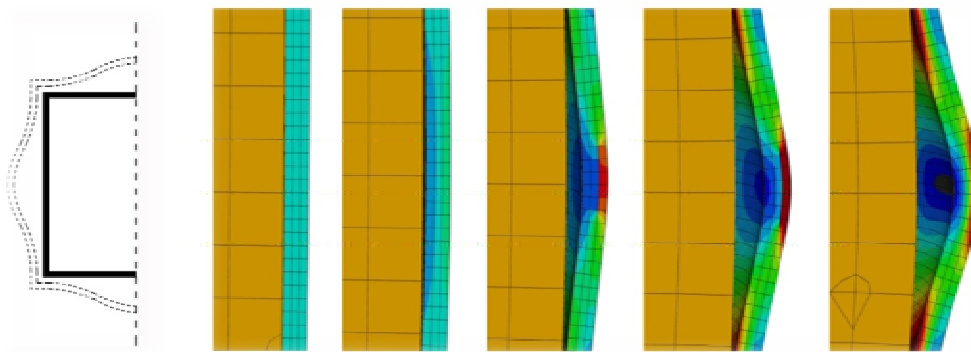

Fig. V.33 Vertical stress evolution in the wall-thickness.
Note how the plate changes from a compressive state into a flexural state.

The evidence of a lack of confinement effect in those areas of the core which correspond to the deformed parts of the plates is that concrete does not follow the deformed shape of the tube, contrarily to the case of circular sections[12]. The behavior of steel differs from that of concrete, and contact of the interface vanishes really fast when local buckling occurs. The transition of the plate from compression to bending is detailed in figure V.34; it is curious to see how the tube is capable of keeping a global compressive response, although it is clearly subjected to bending.
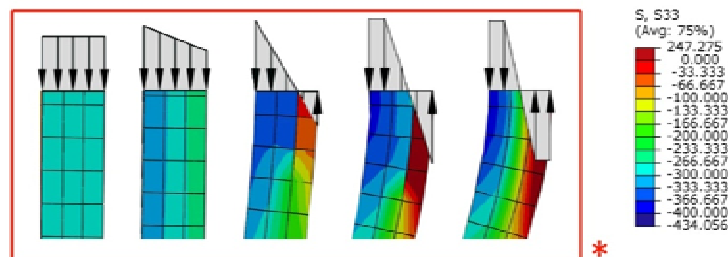

Fig. V.34 Transition from a tensional compressive state to bending [MPa].
The plates show a low flexural rigidity, compared with the axial response.

The sequence presented before belongs to the period between points D and E of figure V.35, during what the section shows an enhancement of strength owing to plastic hardening behavior. In this figure, the averaged vertical component of stress is compared to the homologous transversal component; it can be easily noted that while the first decreases from point **b** to **c**, the latter grows considerably up, remaining almost constant from that point. Although bending of the plate has a clear influence on the ductility of the section [much shorter than in circular CFT sections], during the period between points **c** and **d** the tube does show a hardening period despite its deformed shape.
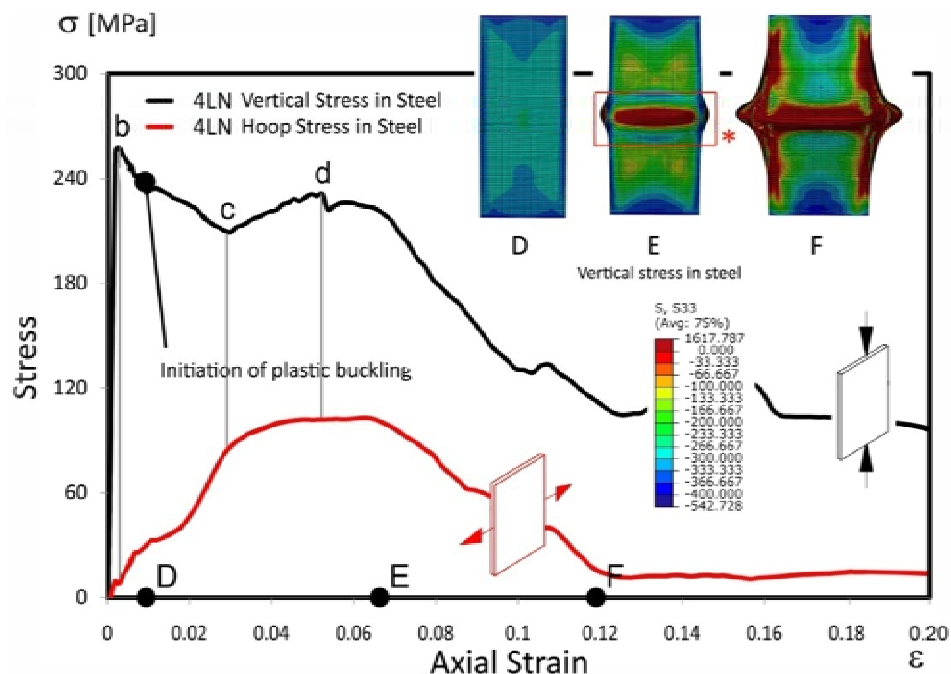

Fig. V.35 Comparison between averaged vertical and transversal stresses of the tube.

---

[12] See the gap existing between steel and concrete in figure V.33.

Diagrams obtained from the FE analysis of specimen 4LN.
Images on the right correspond to the distribution of vertical stress in the tube, [MPa].

Although the behaviors of the two components in a CFT section go usually hand in hand [due to logical reasons of unity], in some cases –especially those cases concerning to large deformation axial loading- they work separately. This is the case of concrete and steel beyond point **d** of figure V.35. The steel tube collapses by showing a significant rate of ductility [both stress components diminishes], and concrete shows a smooth tensional descent until a final value of residual stress. This behavior is thanks to the rigidity of the edges of the tube: despite being notably deformed at advanced stages of strain, the four edges of the tube preserve certain confinement effect on the core owing to the natural arch effect, even in the vertical axis. This phenomenon allows to the damaged concrete having a smooth collapse [see figure V.36].
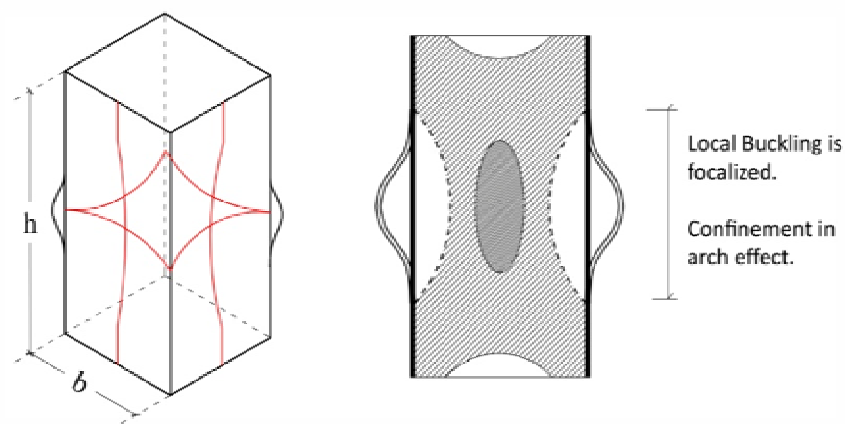

Fig. V.36 Confinement of the core is kept, despite local buckling of the tube.
The stress distribution of confinement on concrete core occurs in arch effect.

As it has been mentioned in figure V.27, the post-collapse behavior shows a significant descending slope owing to the elevated deformability of the plates, but also due to considering the true stress-strain curve for steel under compression only. The use of the compressive true stress-strain curve allows getting accurate load-strain curves under compression analyses, but it leads to undervalue the post-collapse behavior. This phenomenon has been determined in the load-strain curve of Fig. V.27, but it can be perfectly quantified through the sequence presented in figure V.37, where tensional states of the tube are described in terms of tension or compression:
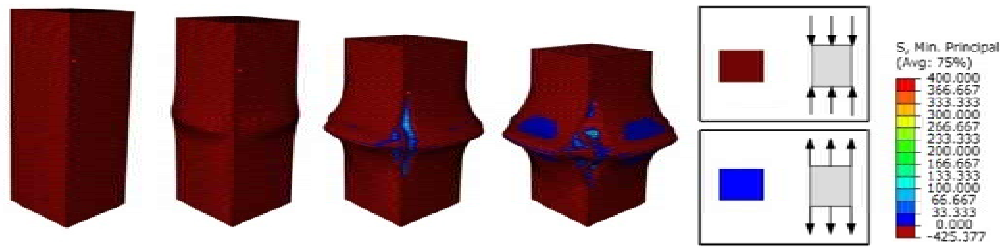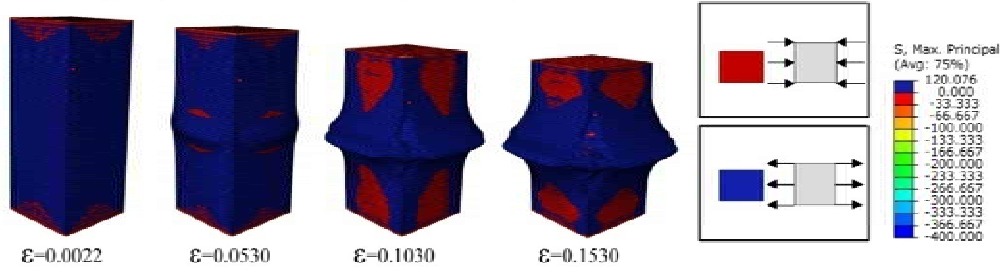
Fig. V.37 Evolution of tensile/compressive stresses in the tube wall.
The two sequences belong to vertical [first] and lateral stresses [second], in MPa.

The combination of these two sequences leads to the simplification of figure V.38, where three basic different states are determined. The first, in red, belongs to biaxial compression; the second, in violet, corresponds to the axially compressed and transversally tensioned area; and finally, the third, in blue, refers to those parts of the tube subjected to pure biaxial tensile states.
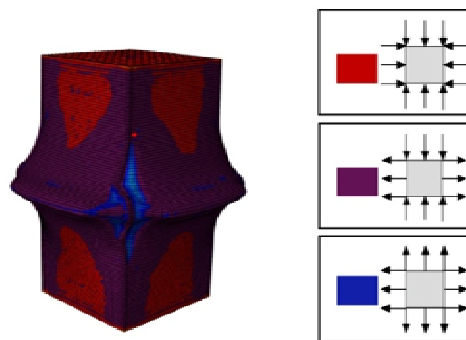
Fig. V.38 Three different stress states can be detected in the steel tube after the collapse.
Those blue areas correspond to a biaxial tensile state.

The appearance of some areas subjected to biaxial tensile stress states leads to a dramatic reduction of the thickness of the plate at these points; that phenomenon must involve the true stress-strain curve for steel under tension, which enhances the capacity of steel at advanced percentages of deformation, owing precisely to the reduction of the thickness of the sample. Note in figure V.38 how this reduction is evident, in comparison with a compressed area.
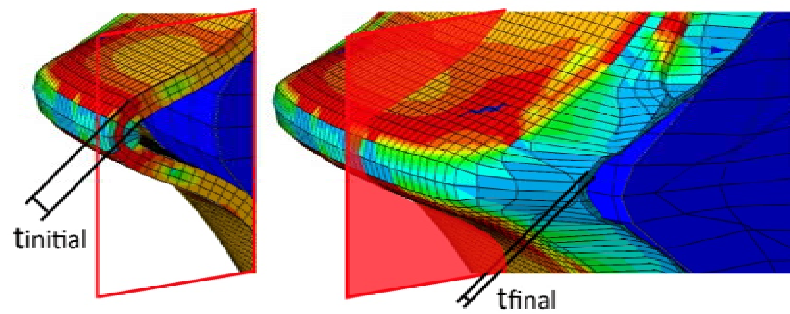
Fig. V.39 The reduction of the plate thickness in some areas accelerates the collapse.
This reduction is enhanced by the use of the true stress-strain curve under compression.

The consideration of the true stress-strain curve for compression, combined with some areas with a clear reduction of thickness implies a more abrupt collapse.

In the diagrams shown in figure V.40, vertical and lateral averaged stresses of the core are also represented. Although a slight increment of strength is observed in the first elastic range, the most significant growth is detected in the hardening period of steel. Note that this spectacular escalation overlaps with the maximum value of lateral stress of the tube, as it is shown in figure V.35. Once the tube has been deformed completely in the middle of the height, concrete follows its own way absorbing part of the load, and filling the existing gap between components.
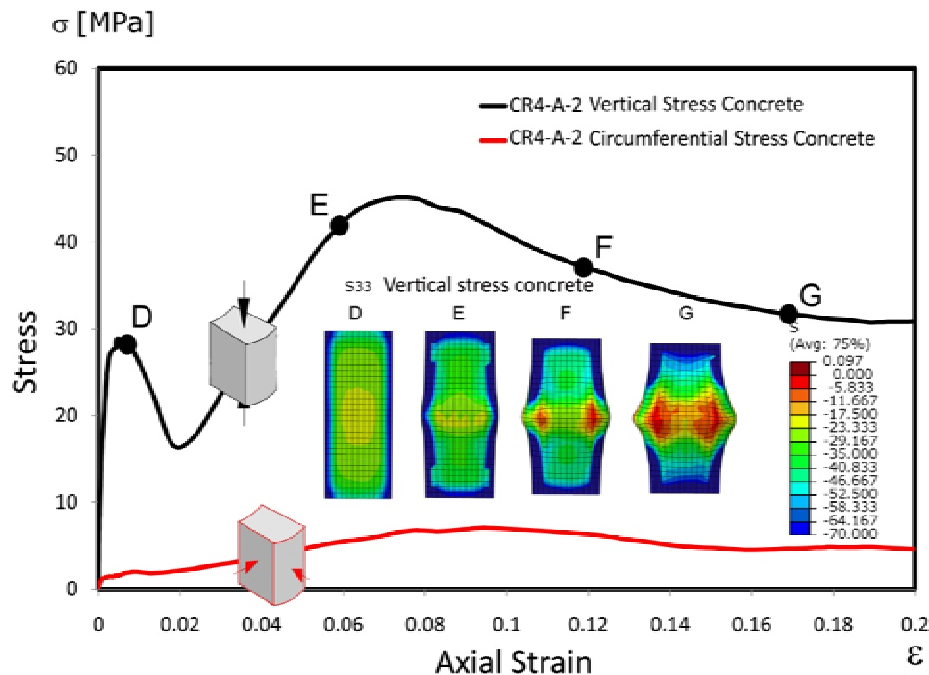

Fig. V.40 General diagrams of averaged vertical and radial stresses of concrete core.
Results coming from the FE analysis of specimen 4LN, expressed in MPa.

As concrete fills in the gap caused by the deformed shape of the tube, confinement on outer areas of the core tends to diminish quickly to zero [see figure V.35], although in the centre, the confinement of concrete is kept thanks to the arch effect derived from the rigidity of the edges.
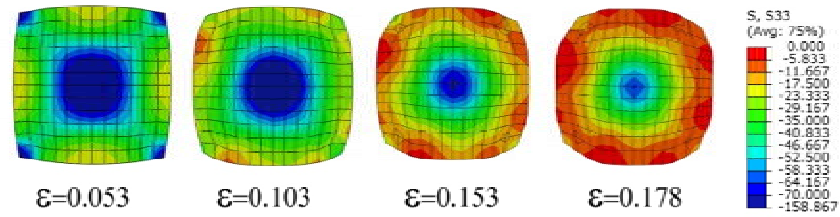
$\varepsilon=0.053$ $\qquad$ $\varepsilon=0.103$ $\qquad$ $\varepsilon=0.153$ $\qquad$ $\varepsilon=0.178$

Fig. V.41 Evolutionary sequence of vertical stress in concrete core after the peak of load.
Results coming from the analysis of specimen 4LN, expressed in MPa.

Figure V.42 shows the loading path of averaged vertical and transversal stresses of the tube on the biaxial plane. Differences with the described circular section shown in figure V.19 are evident; although the first period coincides in both cases [up to point b], we can see how the transition from the first elliptical von Mises surface to the extended hardening surface [concentric to the first] is not really possible. The high deformability shown by the plates does not allow making full profit of the hardening stress of steel.
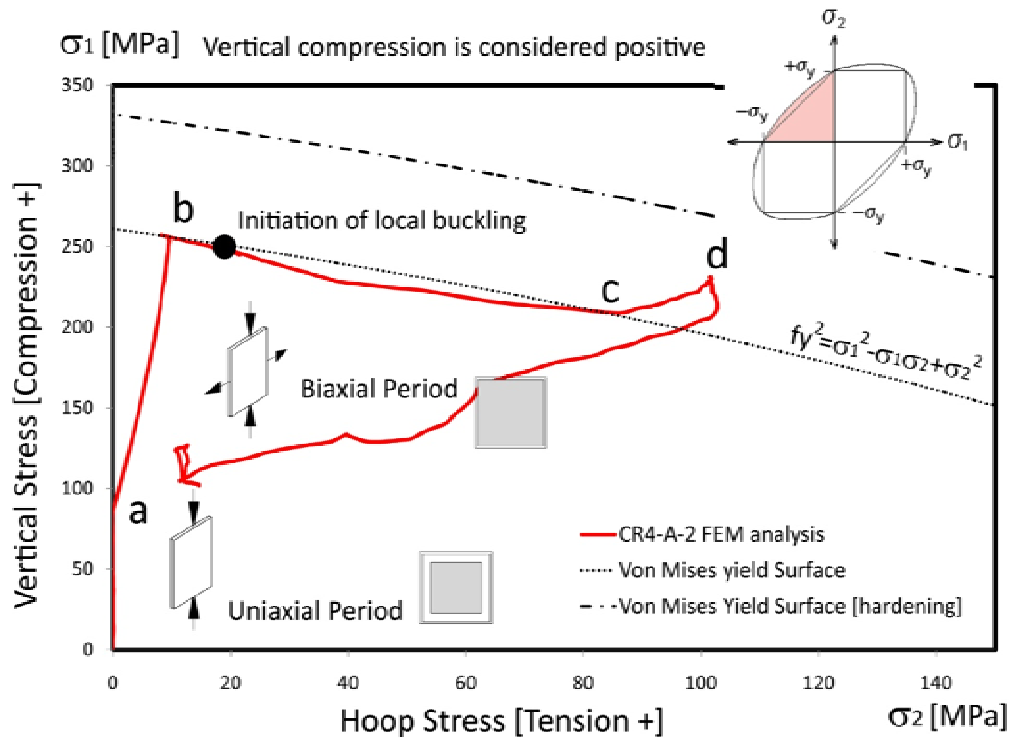

Fig. V.42 Loading path of steel on the biaxial stress plane.
Both uniaxial and biaxial stress states can be detected.

5.4.4 Evolutionary compressive damage description of concrete core.

Deformability of the plates has a clear effect on the evolutionary damage process of concrete. Although few differences can be observed between the damage process of circular and rectangular sections, it is evident that the early buckling of the plates leads irremediably to a quicker advance of the crushing process in concrete. Note how between the first and the second frame in the sequence of figure V.43 there is a huge progress of compressive damage, while in the same interval corresponding to the sequence of figure V.22, this advance is much smoother.
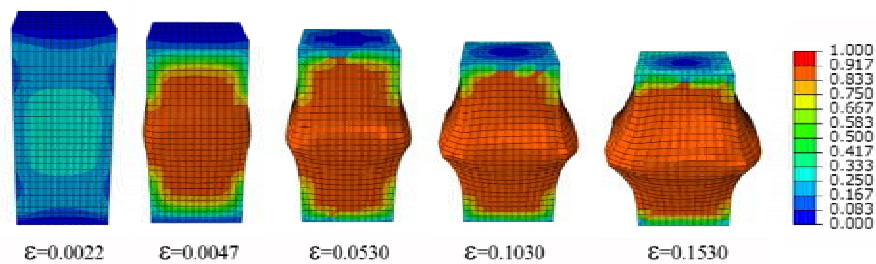

Fig. V.43 Evolutionary sequence of compressive damage ratio in concrete core.
Results coming from the FE analysis of specimen 4LN.

It is important to highlight that, while crushing in circular CFT sections spreads outwards uniformly from the centroid, this process in square-shaped tubes initiates at the mid-height of the specimen growing up towards to the bases. This fact is accelerated by the elevated deformability of the plates again.

5.4.5 Description of the ductility and mode of failure.

As it has been widely explained, thick-walled square tubes show a much less ductility than their circular counterparts; according to the previous sections, the combination of a lack of flexural stiffness of the plates together with a unequal response to volumetric expansion of the core, entails an important diminution of ductility in these last sections. The difference is quite notorious: from a ultimate strain of 0.17 in CR4-A-4 [circular section analyzed before], to a value of 0.06 for 4LN.

Besides, the mode of failure of square-shaped CFT sections is much simpler than that of circular sections, and clearly premature. While in the latter group, the mode of failure follows the shape in "elephant foot", in the first group the collapse goes after the natural bending of plates; this is the reason why the two failure modes are different. Steel in circular CFT sections keeps on totally compressed until advanced rates of strain, from which point the tube collapses by following local buckling phenomena in the nearby of the loaded edges. Really different is the case of square-shaped specimens, in which the tube walls combine compression and bending much earlier.

Thus, the collapse of the steel tube in square-shaped sections spreads from the mid-heigth of the specimen, while this failure in case of rectangular sections occurs at different heights. After the collapse of steel, the entire responsibility of loading lies in the core; thus, as the load transferred to the tube is well above the load-bearing capacity of the damaged concrete. Then, concrete of the core follows the collapse of the tube too.
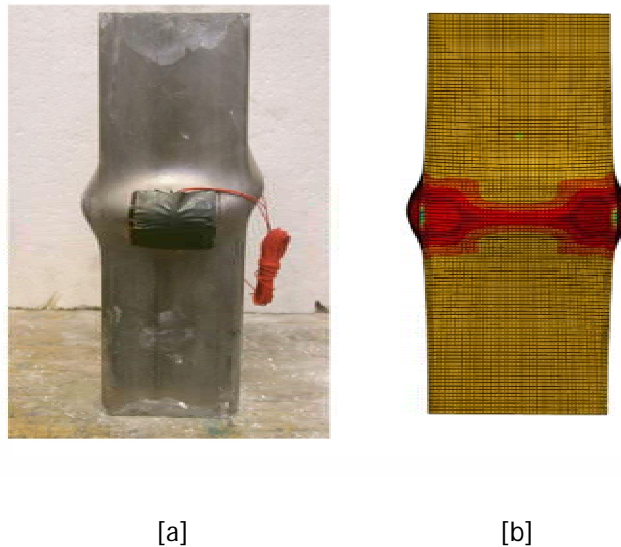
[a]   [b]

**Fig. V.44 Comparison of the mode of failure, coming from an experimental test [a]
and from the FE analysis [b].**

Full coincidence is observed in the mode of failure between the specimens tested by Lam and
Gardner (Lam, et al., 2008) and the deformed shape from the FE analysis.

5.4.6 Evolutionary description of contact pressure between components.

Contact pressure describes the interaction between the two components with surprising accuracy.
As it is shown in figure V.45, those parts of the core which are most loaded are the four edges,
providing to concrete a distribution of confinement in arch effect on the cross-sectional plane [see
figure V.31]. Note that as deformation progresses, pressure to the core increases even in central
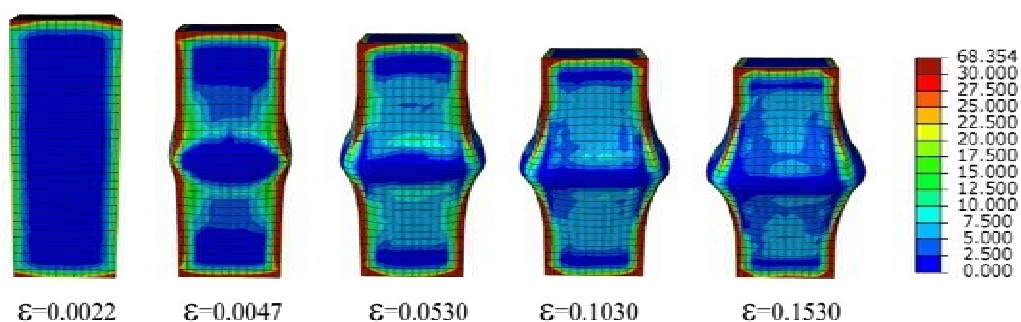parts of rectangular tubes.

$\varepsilon=0.0022$ $\varepsilon=0.0047$ $\varepsilon=0.0530$ $\varepsilon=0.1030$ $\varepsilon=0.1530$

Fig. V.45 Evolutionary sequence of contact pressure on concrete core.
Those parts which are most loaded are the four edges.

In the first step of the previous sequence [coinciding approximately with the peak of load], the
confinement effect is entirely provided by the four rigid edges of the tube since the rest of the plates
are not uniformly pressed. When local buckling appears in the mid-height of the sample, the two
materials starts separating and the contact pressure quickly vanishes [see the central parts of
rectangular plates].